Tran-SET

Transportation Consortium of South-Central States

Solving Emerging Transportation Resiliency, Sustainability, and Economic Challenges through the Use of Innovative Materials and Construction Methods: From Research to Implementation

Self-Healing Concrete using Encapsulated Bacterial Spores in a Simulated Hot Subtropical Climate

Project No. 18CLSU02

Lead University: Louisiana State University

Collaborative Partners: Louisiana Transportation Research Center

Final Report

August 2019

Disclaimer

The contents of this report reflect the views of the authors, who are responsible for the facts and the accuracy of the information presented herein. This document is disseminated in the interest of information exchange. The report is funded, partially or entirely, by a grant from the U.S. Department of Transportation's University Transportation Centers Program. However, the U.S. Government assumes no liability for the contents or use thereof.

Acknowledgements

The authors would also like to acknowledge the laboratory support from the Louisiana Transportation Research Center, the technical expertise and feedback of Dr. Gary King. The authors would also like to acknowledge the work and contributions from Ahsennur Soysal.

TECHNICAL DOCUMENTATION PAGE

1. Project No.	2. Government Accession No.	3. Recipient's Catalog No.
18CLSU02		

4. Title and Subtitle	5. Report Date
Self-Healing Concrete using Encapsulated Bacterial Spores in a Simulated Hot Subtropical Climate	Aug. 2019
	6. Performing Organization Code

7. Author(s)	8. Performing Organization Report No.
PI: Marwa Hassan https://orcid.org/0000-0001-8087-8232 Co-PI: Jose Milla https://orcid.org/0000-0001-9144-8545 Co-PI: Tyson Rupnow https://orcid.org/0000-0002-5487-3873 GRA: Ahsennur Soysal https://orcid.org/0000-0003-4702-2154	

9. Performing Organization Name and Address	10. Work Unit No. (TRAIS)
Transportation Consortium of South-Central States (Tran-SET) University Transportation Center for Region 6 3319 Patrick F. Taylor Hall, Louisiana State University, Baton Rouge, LA 70803	**11. Contract or Grant No.** 69A3551747106

12. Sponsoring Agency Name and Address	13. Type of Report and Period Covered
United States of America Department of Transportation Research and Innovative Technology Administration Louisiana Transportation Research Center 4101 Gourrier Ave., Baton Rouge, LA 70808	Final Research Report Mar. 2018 – Mar. 2019
	14. Sponsoring Agency Code

15. Supplementary Notes

Report uploaded and accessible at Tran-SET's website (http://transet.lsu.edu/)

16. Abstract

Bacterial concrete has become one of the most promising self-healing alternatives due to its capability to seal crack widths through microbial induced calcite precipitation (MICP). In this study, two bacterial strains were embedded at varying dosages (by weight of cement) in concrete. Beam specimens were used to identify the maximum crack-sealing efficiency, while cylinder samples were used to determine their effects on the intrinsic mechanical properties, as well as its stiffness recovery over time after inducing damage. The concrete specimens were cured in wet-dry cycles to determine their feasibility in Region 6. The results showed that the specimen groups with the highest calcium alginate concentrations (including the control specimens with embedded alginate beads but no bacteria) resulted in higher increases in stiffness recovery. Similarly, the beam samples containing alginate beads (also including the Control 3%C specimen group) had superior crack-healing efficiencies than the control samples without alginate beads (Control NC). This was attributed to the fact that the alginate beads act as a reservoir that can further enhance the autogenous healing capability of concrete. Overall, further research is recommended to verify whether the promising results reported in the literature (relating to self-healing mortar) correlate with concrete proportionally. In addition, there is a need to explore the factors that can maximize the self-healing mechanism of bio concrete through MICP, whether an alternative encapsulation mechanism, nutrient selection, curing regime, or bacterial strain is desired.

17. Key Words	18. Distribution Statement
Self-healing concrete, bacteria, MICP, microbial induced calcite precipitation, spores, bio-concrete, healing agent, biomineralization	No restrictions. This document is available through the National Technical Information Service, Springfield, VA 22161.

19. Security Classif. (of this report)	20. Security Classif. (of this page)	21. No. of Pages	22. Price
Unclassified	Unclassified	40	

Form DOT F 1700.7 (8-72) **Reproduction of completed page authorized.**

SI* (MODERN METRIC) CONVERSION FACTORS

APPROXIMATE CONVERSIONS TO SI UNITS

Symbol	When You Know	Multiply By	To Find	Symbol
		LENGTH		
in	inches	25.4	millimeters	mm
ft	feet	0.305	meters	m
yd	yards	0.914	meters	m
mi	miles	1.61	kilometers	km
		AREA		
in^2	square inches	645.2	square millimeters	mm^2
ft^2	square feet	0.093	square meters	m^2
yd^2	square yard	0.836	square meters	m^2
ac	acres	0.405	hectares	ha
mi^2	square miles	2.59	square kilometers	km^2
		VOLUME		
fl oz	fluid ounces	29.57	milliliters	mL
gal	gallons	3.785	liters	L
ft^3	cubic feet	0.028	cubic meters	m^3
yd^3	cubic yards	0.765	cubic meters	m^3
		NOTE: volumes greater than 1000 L shall be shown in m^3		
		MASS		
oz	ounces	28.35	grams	g
lb	pounds	0.454	kilograms	kg
T	short tons (2000 lb)	0.907	megagrams (or "metric ton")	Mg (or "t")
		TEMPERATURE (exact degrees)		
^oF	Fahrenheit	5 (F-32)/9 or (F-32)/1.8	Celsius	^oC
		ILLUMINATION		
fc	foot-candles	10.76	lux	lx
fl	foot-Lamberts	3.426	$candela/m^2$	cd/m^2
		FORCE and PRESSURE or STRESS		
lbf	poundforce	4.45	newtons	N
lbf/in^2	poundforce per square inch	6.89	kilopascals	kPa

APPROXIMATE CONVERSIONS FROM SI UNITS

Symbol	When You Know	Multiply By	To Find	Symbol
		LENGTH		
mm	millimeters	0.039	inches	in
m	meters	3.28	feet	ft
m	meters	1.09	yards	yd
km	kilometers	0.621	miles	mi
		AREA		
mm^2	square millimeters	0.0016	square inches	in^2
m^2	square meters	10.764	square feet	ft^2
m^2	square meters	1.195	square yards	yd^2
ha	hectares	2.47	acres	ac
km^2	square kilometers	0.386	square miles	mi^2
		VOLUME		
mL	milliliters	0.034	fluid ounces	fl oz
L	liters	0.264	gallons	gal
m^3	cubic meters	35.314	cubic feet	ft^3
m^3	cubic meters	1.307	cubic yards	yd^3
		MASS		
g	grams	0.035	ounces	oz
kg	kilograms	2.202	pounds	lb
Mg (or "t")	megagrams (or "metric ton")	1.103	short tons (2000 lb)	T
		TEMPERATURE (exact degrees)		
^oC	Celsius	1.8C+32	Fahrenheit	^oF
		ILLUMINATION		
lx	lux	0.0929	foot-candles	fc
cd/m^2	$candela/m^2$	0.2919	foot-Lamberts	fl
		FORCE and PRESSURE or STRESS		
N	newtons	0.225	poundforce	lbf
kPa	kilopascals	0.145	poundforce per square inch	lbf/in^2

TABLE OF CONTENTS

LIST OF FIGURES

LIST OF TABLES

ACRONYMS, ABBREVIATIONS, AND SYMBOLS

ASTM	American Society for Testing and Materials
ASCE	American Society of Civil Engineers
B or *B. pseudofirmus*	*Bacillus Pseudofirmus*
CN	Calcium Nitrate
CW	Crack Width
DN or *D. nitroreducens*	*Diaphorobacter Nitroreducens*
EDS	Energy Dispersive Spectroscopy
LSD	Least Significant Difference
LTRC	Louisiana Transportation Research Center
MICP	Microbial Induced Calcite Precipitation
RH	Relative Humidity
SD	Standard Deviation
SEM	Scanning Electron Microscope

EXECUTIVE SUMMARY

Concrete is one of the most commonly used construction materials in the world, due to its relatively low cost and high compressive strength. However, its weakness in tension makes it susceptible to cracking and thereby exposes any steel reinforcement to harmful agents that cause corrosion. Several techniques are currently used for crack-sealing but with the current funding limitations, it is especially harder to afford the costly and labor-intensive maintenance and repair services needed to extend a structure's service life.

Bacterial concrete has become one of the most promising self-healing alternatives due to its capability to seal crack widths up to 1 mm by reacting directly with the cementitious matrix to form calcium carbonate. It is developed by adding alkali-resistant bacterial spores, which do not impose hazards to human health, in the concrete mixing process. Furthermore, bacterial induced calcium carbonate precipitation is directly compatible with Portland cement materials and promotes economic and environmental benefits by increasing durability and water-tightness in concrete. The success of the self-healing reaction generally depends on the presence of water, a mineral precursor compound and/or nutrient for the bacteria, and a calcium source. Wet-dry cycles have been identified as the ideal curing conditions to maximize the bacterial concrete's healing capacity. Thus, this application has potential for implementation in Region 6.

In this study, the authors followed an encapsulation procedure to immobilize and protect the bacteria strains during the concrete mixing process. Two bacterial strains, namely *Bacillus pseudofirmus* and *Diaphorobacter nitroreducens*, were added at varying dosages (by weight of cement) in concrete. Beam specimens were used to identify the maximum crack-sealing efficiency, while cylinder samples were used to determine their effects on the intrinsic mechanical properties, as well as its healing over time after inducing damage. Both the concrete beam and cylinder specimens were cured in wet-dry cycles to determine their feasibility in Region 6.

The influence of the calcium alginate beads on the intrinsic mechanical properties of concrete was explored. In general, lower concentrations of alginate beads did not yield significant differences in compressive strength (at 0.5% by wt. of cement) and modulus of elasticity (at 0.5% and 1.5% by wt. of cement) than the control specimens with no alginate beads embedded.

After overloading the concrete cylinders to inflict damage (at 90% of their ultimate strength), the drop in modulus of elasticity was measured, and the samples were then allowed to heal in wet/dry cycles consisting of 8 hours of water immersion and 16 hours of air drying at a 50% RH room. The specimen groups with the highest calcium alginate concentrations resulted in higher increases in stiffness recovery. Interestingly, this observation also applied with the control specimens embedded with 3% calcium alginate beads without bacteria.

The self-healing efficiency was also monitored on cracked concrete beams over a period of 28 days. After measuring the crack widths of damaged beams over time, it was evident that those samples containing alginate beads had superior self-healing efficiencies than the control samples without alginate beads (Control NC). However, it is important to note that the Control 3%C group (containing alginate beads with nutrients but no bacteria) also showed promising results in self-healing. This can be attributed to the fact that the alginate beads act as a reservoir that can further enhance the autogenous healing capability of concrete.

Overall, further research is recommended to verify whether the promising results reported in the literature (relating to self-healing mortar) correlate with concrete proportionally. In addition, there is a need to explore the factors that can maximize the self-healing mechanism of bio concrete through microbial induced calcite precipitation (MICP), whether an alternative encapsulation mechanism, nutrient selection, curing regime, or bacterial strain is desired.

1. INTRODUCTION

Concrete is one of the most commonly used construction materials in the world, where approximately 4 billion cubic meters of concrete are produced annually. While strong in compression, its weakness in tension makes it susceptible to cracking and thereby exposes any steel reinforcement to harmful agents that may cause corrosion. The latest infrastructure report card from the American Society of Civil Engineers has determined that the US civil infrastructure is poorly maintained, with insufficient funds to improve roadways and bridges throughout the nation, thus earning a D+ grade. Inadequate funding has steadily increased the backlog of new construction, repair and maintenance, up to $836 billion for highway and bridge infrastructure *(1)*. As such, there is a clear need to increase the durability of construction materials to alleviate the backlog and the costs associated with repair and maintenance.

One possible solution is to develop self-healing concrete materials to prevent the ingress of corrosive agents that deteriorate the steel reinforcement. In recent years, self-healing materials have gained significant research attention as they increase durability and alleviate the ever-increasing maintenance costs for concrete infrastructure. During a cracking event, a self-healing mechanism is triggered by any combination of (a) environmental conditions; (b) chemical agents; and/or (c) biological agents to produce a material to seal the cracks *(2)*. Examples of self-healing materials include Engineered Cementitious Composites (ECCs), the introduction of expansive agents, mineral admixtures, and microencapsulated healing agents embedded in concrete. These strategies have shown promising results in sealing hairline cracks autonomously in the presence of moisture.

Microencapsulation of healing agents has been proven to be an effective approach as it provides a localized response to damage. Hence, as concrete cracks, the microcapsules rupture due to tensile stresses and release the healing agent which reacts with the cementitious matrix *(3-5)*. Promising results have also been reported in recent years by incorporating microorganisms capable of precipitating calcium carbonate to seal cracks autonomously, where the maximum crack widths healed are significantly larger than the control specimens *(6-11)*. Due to concrete's harsh environment, however, research studies have found that bacterial protection is essential to significantly increase the efficiency of this technology *(12)*. This can be achieved by encapsulating bacteria or impregnating bacteria into highly absorptive materials such as expanded clays or diatomaceous earth *(13-14)*.

The success of the self-healing reaction depends on the bacteria's metabolic pathway, as this would determine the optimal nutrients and environmental conditions to induce calcite precipitation *(15)*. The initiation of microbial induced calcite precipitation (MICP) depends on the type of organic precursor used, the bacterial strain's productivity, the availability of nutrients, and a calcium source. The curing conditions also influence the extent of self-healing activity, where exposure to free water has been identified as a critical factor *(16)*. However, studies have shown that wet-dry cycles may yield higher healing efficiencies than samples cured in water-immersion or 95% relative humidity chambers *(3,7)*. Thus, this application has potential for implementation in humid subtropical climates in Region 6.

In this study, the authors aim to develop an encapsulation procedure that will allow for testing two bacterial strains in concrete. Concrete beams will be used to identify the crack-sealing efficiency and potential crack width limitations, while concrete cylinders will be used to determine their effects on the intrinsic mechanical properties, as well as its stiffness recovery over time after

inducing damage. Three different levels of microencapsulated bacteria (at 0.5%, 1.5%, and 3.0% by weight of cement) will be tested to determine the optimal concentration needed, balancing the observed self-healing efficiency with any potential impacts on the intrinsic concrete properties. In addition, the concrete specimens will be cured using wet-dry cycles to evaluate their feasibility for implementation.

2. OBJECTIVES

The research project's objective is to evaluate the performance of two bacterial strains, namely *Bacillus pseudofirmus* and *Diaphorobacter nitroreducens*, for self-healing concrete applications through microbial induced calcite precipitation (MICP). Three different levels of encapsulated bacteria (at 0.5%, 1.5%, and 3.0% by weight of cement) will be tested to determine the optimal concentration needed, balancing the observed self-healing efficiency with any potential impacts on the intrinsic concrete properties. These will be compared with the results from two control groups: the main control group which does not include any bacteria or nutrients, and the second control group which consists of 3% encapsulated nutrients (by weight of cement) but no bacteria. Their effect on concrete's properties, stiffness recovery, and crack-sealing was evaluated after subjecting the damaged concrete specimens in wet-dry cycles consisting of 8 hours of water-immersion and 16 hours of air drying at a 50% relative humidity room.

3. LITERATURE REVIEW

Concrete is the most widely used material in construction worldwide due to its compressive strength and relatively low cost. However, its low tensile strength and susceptibility to cracking often compromise its durability, performance, and life span. Although concrete has autogenic capacity to heal the cracks, the size of the cracks that can undergo autogenous healing depends on the exposure conditions and remains below 0.17 mm *(17)*. Even though crack widths smaller than 0.2 mm do not impose a structural threat, infiltration of chlorides, sulphates, and acids result in corrosion of concrete's steel reinforcement, or expansion of the hardened cement paste, which can then lead to catastrophic structural damage. Enormous expenses are required for maintenance and repair of cracks. It is estimated that the United States spends $4 billion annually on concrete highway bridges as an outcome of reinforcement corrosion *(18)*.

Self-healing materials have gained significant research attention in recent years, due to their ability to increase durability and alleviate the ever-increasing maintenance costs for concrete infrastructure. During a cracking event, a self-healing mechanism is triggered by any combination of environmental conditions, chemical agents, and/or biological agents to produce a material to seal the cracks *(2)*. Examples of self-healing materials include the introduction of mineral admixtures in concrete, microencapsulation of healing agents embedded in concrete, and bacterial concrete. These approaches have shown promises in sealing hairline cracks autonomously in the presence of moisture.

Microencapsulation of healing agents has been proven to be an effective approach as it provides a localized response to damage. It's a process in which substances are entrapped or immobilized in a coating or polymer matrix in the form of beads (as done in this study) or capsules/core-shell systems (which involve a secondary membrane layer). Microencapsulation is used widely for the protection and delivery of chemical substances, enzymes, vitamins, or whole cells or microbes in diverse biomedical or technological fields such as drug delivery, tissue engineering, or probiotic food amendment. While beads have the encapsulated material distributed throughout the matrix, capsules consist of a defined core containing the encapsulated material that is surrounded by a secondary shell membrane *(19)*. The matrix is usually comprised of a water-soluble porous polymer which serves as protection or a barrier through which only small specific compounds can diffuse, while larger molecules such as proteins or cells remain immobilized.

During a cracking event in concrete or mortar, the microcapsules will rupture due to tensile stresses and release the healing agent to react with the cementitious matrix. Eight key factors that affect self-healing by encapsulation are as follows: (i) robustness during mixing, (ii) probability of cracks encountering the capsules, (iii) curing time and condition, (iv) effect of empty capsules on concrete strength, (v) controllability of release of healing agent, (vi) stability of healing agent, (vii) sealing ability and recovery of durability and strength of concrete matrix (as a result of self-healing), and (viii) repeatability of self-healing action *(5)*.

If bacteria are selected as a healing agent, it will initiate the MICP process to seal the cracks, provided its environmental and nutrient requirements are satisfied. Each bacterium has a very specific and narrow water activity for optimum metabolism and growth. More recent studies show that *Bacilli* and closely related bacteria are moderately tolerant of dry conditions. For applications of bio self-healing concrete, it is necessary to design a matrix capable of shielding the cells in a concrete environment. One of the main issues with direct incorporation of bacterial cells into the

concrete mixture is the mixture's harsh environment and concrete's high pH (which is about 12 pH). The encapsulation of bacterial cells into a polymeric matrix such as calcium alginate (Ca-alginate) is a promising example of this kind of solution. Furthermore, with encapsulation there is potential for the encapsulated bacterial cells to be separated and re-used. However, the concentrations of Na-alginate and $CaCl_2$ used to form Ca-alginate significantly influence the permeability and the mass transfer capability of the beads and, consequently, the bio-mineralization of $CaCO_3$ are affected *(9).*

3.1. Microbial Induced Calcite Precipitation

Concrete has a remarkable capability to naturally repair cracks in the presence of moisture (and the absence of tensile stresses), through a process known as autogenous healing. While autogenous healing can take place through further hydration of unreacted cementitious materials or swelling of calcium-silica-hydrate, the most common form of autogenous healing is attributed to the precipitation of calcium carbonate crystals on the cracked surfaces *(2)*. However, this process is limited to crack widths under 0.17 mm *(17).* Thus, research efforts have focused on improving concrete's self-healing capacity. Studies have shown that microbial induced calcite precipitation (MICP) has been found to be a promising approach *(2-15)*. Through this method, when a crack occurs, the bacteria induces calcium carbonate ($CaCO_3$) precipitation to seal cracks in the presence of moisture *(9).*

Biomineralization in the form of MICP refers to the process where calcium carbonate minerals are formed from a supersaturated solution in the presence of microorganisms. During MICP, bacterial cells able to secrete carbonate ions (CO_3^{2-}) that react with a calcium-rich solution to precipitate calcium carbonate, which is insoluble in water. The species of the bacterial cells used can lead to the production of different phases of calcium carbonate. These include $CaCO_3$ anhydrous polymorphs such as calcite, aragonite and vaterite, as well as hydrated crystalline phases such as monohydrocalcite ($CaCO_3 \cdot H_2O$), hexahydrocalcite ($CaCO_3 \cdot 6H_2O$), and amorphous calcium carbonate (ACC). Calcite and vaterite are the most common polymorphs, while vaterite is a minor, metastable and transitional phase during calcite formation. Calcite is the most thermodynamically stable polymorph of calcium carbonate and the primary product formed in most MICP reactions *(20)*.

3.2. Metabolic Pathways

Several bacteria species have been tested in mortar or concrete specimens for self-healing processes, including *Bacillus megaterium*, *Bacillus subtilis*, *Bacillus aerius*, *Sporosarcina pasteurii*, and *Bacillus sphaericus*, among others. Ideally, the bacterial strains studied must be alkaliphiles (a class of bacteria that can survive in alkaline environments, usually between a pH of 8.5 to 11) for concrete applications. Their efficiency in self-healing greatly depends on the metabolic process in which calcium carbonate is precipitated, where virtually all the bacterial strains studied in concrete achieve MICP through three main pathways. The details of these pathways are described below.

3.2.1. Urea Hydrolysis

The most commonly studied MICP pathway for concrete applications has been urea hydrolysis via the bacteria's urease enzyme in a calcium rich environment. Typical ureolytic strains embedded in concrete are *Bacillus pasteurii*, *Bacillus sphaericus*, and *Bacillus megaterium* for self-healing

applications *(21)*. The rate of biomineralization or calcite precipitation reaction is influenced greatly by the bacteria's urease activity, and the availability of urea (precursor), yeast extract (nutrient), water, and calcium. Indeed, oxygen and yeast extract are essential elements that influence the germination and outgrowth of bacterial spores. This is particularly important to maintain the bacteria's ureolytic activity to keep precipitating calcium carbonate.

The MICP pathway is activated when urea is decomposed into ammonium and carbonate ions, where the carbonate reacts with the calcium ions available within the cementitious matrix to produce calcium carbonate. The bacterial activity can be quantified by measuring the amount of urea decomposed based on the total ammonium nitrogen present, since one mole of urea produces two moles of ammonium. However, it is important to note that the production of ammonium raises concerns for its detrimental effects in concrete since it contributes to calcium hydroxide leaching, similar to an acid attack *(22-24)*. Also, oxidation of urea to nitrous acid, and then nitric acid via ureolytic bacteria can lead to severe corrosion of building materials *(18)*. Another potential drawback arises when admixing yeast extract in concrete, since it has been shown to be detrimental to the compressive strength, and acts as a retarder to the cement hydration. Therefore, a limited amount of nutrients would be available within the cementitious matrix to avoid adverse effects in concrete. *(6, 25-26)*.

3.2.2. Conversion of Organic Salts

This process involves a metabolic conversion of organic salts through bacterial respiration to produce carbon dioxide. In the presence of water, such produced carbon dioxide dissolves and forms carbonate ions. Therefore, in a calcium rich environment, the carbonate ions react with the calcium ions to precipitate calcium carbonate in an alkaline environment. In addition, the yield of MICP can be increased further when the carbon dioxide generated through bacterial respiration reacts with the calcium hydroxide in the cementitious matrix to form additional non-soluble, calcite crystals. The success of the self-healing reaction for this pathway depends on the presence of water, oxygen, a calcium source, and the selection of the organic salt or mineral precursor.

Bacterial activity can be quantified by measuring the oxygen consumption of the bacterial culture, given that the metabolic conversion of organic salts requires oxygen to produce carbon dioxide and thus initiate the MICP reaction. Moreover, the mineral precursor selection and concentration is key and ideally, it should not impact the intrinsic concrete properties. Studies have found that nutrients such as peptone, calcium acetate, and yeast extract have negative effects in the compressive strength of cementitious materials. Nevertheless, calcium lactate was found to have no impacts on the early age compressive strength, and in fact showed higher 28-day compressive strength results *(6)*. Successful self-healing has been reported when using *Bacillus cohnii*, *Bacillus pseudofirmus*, and *Bacillus alkalinitrilicus* strains *(6, 13)*. Moreover, the *Bacillus* species tend to show the highest ability to produce $CaCO_3$ in the form of calcite. Specifically, *Bacillus pseudofirmus* has high sporulation, germination extent, and spore survival in cement, with a particularly higher calcite precipitation levels compared to a few other *Bacilli* strains *(18)*.

3.2.3. Nitrogen Reduction

The biological reduction of nitrates occurs when nitrate (instead of oxygen) is used by bacteria to respire. Therefore, during the denitrification of an organic salt, the bacteria produces carbon dioxide, which in an aqueous media yields carbonate that reacts with free calcium to produce calcium carbonate. This addresses one of the limitations found in certain bacterial strains that

'starve' due to minimal oxygen availability, and therefore deters the continuous growth of bacteria to maintain an active and stable calcite precipitation rate *(11, 27)*. Hence, the main benefit to this pathway is that it is adaptable to an environment with and without oxygen. In addition, a common byproduct of the MICP reaction includes nitrite, which can act as a corrosion inhibitor for steel in reinforced concrete *(11)*. The success of the self-healing reaction for this pathway depends on the presence of water, oxygen or nitrate, a calcium source, and the selection of the mineral precursor.

Biomineralization through nitrogen reduction has been investigated for soil reinforcement with *Pseudomonas denitrificans (28)* and *Castellaniella denitrificans (29),* as well as for concrete applications with *Synechococcus* PCC8806 *(30), Pseudomonas aureginosa*, and *Diaphorobacter nitroreducens*. *Synechococcus* PCC8806 is an auto-phototrophic cyanobacterium that precipitates calcium carbonate through photosynthesis and was found to have potential for restoring concrete as it tolerated highly alkaline environments and precipitated calcite that resisted sonication in mortar cubes. *Pseudomonas aureginosa* and *Diaphorobacter nitroreducens* were observed to produce high calcite precipitation and resilience (in its ability to resist dehydration and starvation stress) in minimal nutrient conditions. The bacterial cell suspensions were vacuum impregnated in two protective carriers, expanded clay and granular activated carbon particles, and were subsequently embedded in mortar. After damaging mortar specimens, those specimens containing bacteria reported significant self-healing. Cracks were sealed up to 480 microns in 56 days, and water tightness was regained up to 85% *(27).*

Among the potential nutrients for such nitrogen-reducing strains, calcium nitrate is an excellent candidate for its high compatibility in concrete materials. It is currently used as a commercial, multi-functional concrete admixture, capable of acting as a corrosion inhibitor, a set accelerator, and a long-term compressive strength enhancer *(31)*. In addition, calcium lactate and calcium formate can also be used as the mineral precursors for nitrogen-reducing strains, which means that the nutrient requirements to initiate the MICP reaction do not cause any detrimental effects in the intrinsic concrete properties *(11)*. The bacterial activity can be quantified by measuring the nitrogen dioxide and nitrate concentrations using a compact ion chromatography instrument. In addition, the nitrogen gas produced can be measured with a compact gas chromatographer.

3.3. Encapsulation Procedures

The encapsulation or immobilization of the bacteria agents is crucial for the success of a biological-based self-healing concrete. As such, it is essential that the encapsulation procedure selected is compatible with the bacteria strains and the surrounding cementitious matrix. In addition, the developed microcapsules must survive the strenuous concrete mixing process and protect the bacteria, such that the bacteria are released only during a cracking event. For this reason, the selection of the shell material is key, as it can control the rate of bacteria release (if the shell is porous), the bond between the cement and the capsule, and the robustness of the shell wall for surviving the concrete mixing process. Some of the most commonly used encapsulation procedures in the literature involve an in-situ polymerization of melamine-formaldehyde, or alginate hydrogel beads produced by extrusion dripping. The most straightforward technique for obtaining alginate beads is extrusion dripping of the matrix through a needle into a hardening bath of $CaCl_2$ solution. The agents to be encapsulated (in this case, the bacteria cells and growth nutrients) are typically mixed into a sterilized alginate solution (usually ranges from 1-2%), which is pumped as a droplet chain into a calcium chloride solution bath, where it hardens into hydrogel beads after a short curing time (5-60 minutes) *(32).* Other suitable encapsulation strategies include synthetic or bio-

based super-absorbent polymers, and impregnation in expanded clays, lightweight aggregates, and diatomaceous earth *(3-4, 13-14).*

3.3.1. Polymer Microcapsules

Bacterial spores and microorganisms in vegetative states are compatible with polymer microencapsulation processes as they are able to withstand harsh conditions, such as heat, and lack of water and oxygen. The most commonly used encapsulation preparation process involves interfacial polymerization reaction of a water-in-oil emulsion. Thus, the bacteria (typically incubated in a water-based solution) are dispersed in a non-aqueous liquid with the aid of a surfactant and mechanical agitation of the mixture. As the aqueous droplets are formed, the solution is then heated between 20 and 90 °C, followed by the addition of an acid catalyst to form the polymer shell. Typically, the shell is a water-insoluble material, and can be formed by several polymeric materials such as gelatine, polyurethane, polyolefin, polyamide, polyester, polysaccharide, silicone resins, and chitosan and epoxy resins *(33).*

Wang et al. *(7)* encapsulated a strain of bacterial spores, specifically *Bacillus sphaericus* LMG 22557, for a self-healing mortar application. Melamine-formaldehyde microcapsules were prepared following a patented poly-condensation process *(33).* A concentration of 10^9 cells/g was successfully encapsulated in capsules averaging 5 µm in diameter. Next, the microcapsules were then added to the mortar specimens at varying concentrations (as a percentage by weight of cement) and tested for self-healing after inducing cracks. The results showed that the specimens with encapsulated bacteria spores successfully sealed up to a maximum 970 µm of crack-width and measured up to 10 times lower water permeability than the control specimens.

3.3.2. Vacuum Impregnation

As an alternative to encapsulation, researchers have also proposed embedding the healing agent mixture directly into porous fine aggregates, diatomaceous earth, and expanded clays via vacuum impregnation. Tziviloglou et al. *(3)* incorporated the bacteria-based healing agent into lightweight aggregates, which are produced from materials such as clay, shale, or slate. The vacuum-impregnated lightweight aggregates were then mixed to produce mortar specimens. The results showed that, when subjected to wet-dry cycles, the permeability decreases significantly for cracked specimens containing the healing agent compared to the control specimens. In addition, oxygen consumption and bacterial traces on calcite formations confirmed the bacterial activity on specimens containing the healing agent.

Wiktor and Jonkers *(13)* added bacterial spores of *Bacillus alkalinitrilicus* and calcium lactate into expanded clay particles as a self-healing agent in concrete. Multiple cracks that originally ranged from 0.05 to 1.0 mm were induced, and after 100 days of water-immersion to evaluate self-healing, crack-healing was observed up to 0.46 mm (while the control specimens only showed up to 0.18 mm healing). Diatomaceous earth has also been explored as a potential carrier for bacterial cells, since it is highly porous material made from powdered siliceous sedimentary rock. Thus, Wang et al. *(14)* used diatomaceous earth to immobilize the carbonic anhydrase-producing *Bacillus mucilaginosus* in cement-based materials. The results showed that the cracks formed at early ages were completely healed up to 0.4 mm (with 0.15 to 0.17 mm more healing compared to control specimens).

3.3.3. Hydrogel Beads

Since availability of free water is essential to trigger the bio-based self-healing reaction in concrete, researchers have proposed the use of hydrogels to promote bacterial activity in most environments without human interference. Hydrogels are hydrophilic gels which have networks of polymer chains, capable absorbing water hundreds of times their own weight. Thus, hydrogels can be used to encapsulate the bacterial cell suspension and also act as a water reservoir to enable the MICP reaction. The most common substance used as an encapsulating polymer is sodium alginate due to its biocompatibility, low toxicity, low cost, simplicity of its capsule-forming process, and easiness to obtain. Sodium alginate, commonly found in the cell walls of brown algae, is a linear anionic polysaccharide. During the process, chemical cross-linking occurs between sodium-alginate where sodium ions are exchanged with divalent ions such as Ca^{2+}, forming a stable bio-polymer gel network *(32, 34)*.

Palin et al. *(4)* used calcium alginate hydrogel beads to encapsulate a healing agent mixture consisting of sodium alginate, bacterial spores ($7x10^8$ cells/L), with magnesium acetate and yeast extract as its nutrients. The calcium alginate beads were prepared using a simple extrusion dripping process, where the healing agent mixture is added drop-wise into a gel bath of calcium chloride to enable the cross-polymerization of calcium alginate. Palin's theoretical calculations estimated that 0.112 g of calcium alginate beads can produce 1 mm^3 of calcium carbonate after 14 days of water immersion, thereby demonstrating the potential of such beads for self-healing concrete applications. Palin et al. utilized the extrusion dripping process for the preparation of the hydrogel beads due to its simplicity. A typical set up is shown in Figure 1, where the production of calcium alginate beads is illustrated.

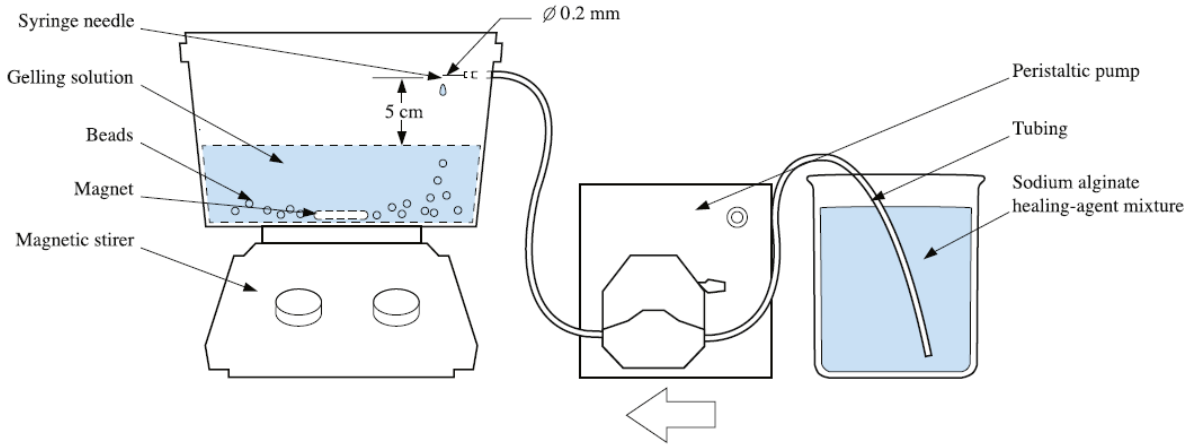

Figure 1. The production of calcium alginate beads using a simple extrusion dripping method (Schematic from Palin et al. *(4)*).

The sodium alginate healing agent mixture is pumped at a flow rate that allows a stable drop-wise addition through the syringe nozzle. As the droplets fall on the gelling solution (typically composed of calcium chloride solution), the solution is gently stirred with a magnetic stirrer. These droplets are then left to cure for 15-30 minutes at room temperature to allow the beads to harden. The main factors that affect the particle size and its distribution are the (i) surface tension of alginate solution, (ii) dripping nozzle's diameter, (iii) concentration of calcium chloride in gelation bath, (iv) curing time of bead in gelation bath, and (v) the mannuronic acid (M) and guluronic acid

(G) ratio that describes the composition of the alginate *(35)*. A summary of the major factors that control the morphology of the alginate beads is shown in Table 1.

Table 1. Production parameters for calcium alginate beads *(38)*.

Process Parameter	Influence on Size	Influence on Morphology
Surface tension of alginate solution	Major	Major
Viscosity of alginate solution	Minor	Major
M/G ratio of alginate	Major	Minor
Dripping tip diameter	Major	Major
Collecting distance	Minor	Major
Concentration of calcium chloride in gelation bath	Major	Major
Stirring rate of gelation bath	Minor	Major
Curing time of beads in gelation bath	Major	Minor
Viscosity of gelation bath	Minor	Major

The technique used by an encapsulator device that resembles extrusion dripping of a matrix via a needle is known as jet vibration, whose main advantages include simplicity, result reproducibility, and high efficiency. Producing homogeneous spherical beads or capsules with a narrow-size distribution can be difficult *(34)*. But devices such as the BÜCHI Encapsulator B-390, as used in this study to microencapsulate bacteria into beads, make this easier and much more efficient to achieve by allowing for the production of a large number of homogenous beads or capsules with a predefined size that ranges from 120-2400 µm (and <5% standard deviation). This jet vibration technique works by pumping and dripping the prepared liquid solution using controlled air pressure as a liquid jet stream through the selected nozzle (ranges from 80-1000 µm) into a polymerization or hardening bath. The jet is broken into equally sized beads/capsules by applying a controlled mechanical vibrational frequency (at a defined amplitude) to the liquid, with one droplet formed per hertz of frequency applied. For the BUCHI Encapsulator, this force is applied by vibrating the polymer liquid in a chamber (bead producing unit) before it is extruded through a selected nozzle, shown in Figure 2. To prevent coalescence of the droplets during jet break-up and/or when entering the gelling bath, an electrical charge is induced onto the surface of the droplets as they pass between the nozzle and an electrode using an electrostatic voltage system. The size of the produced droplets and the rate of production are mainly dependent on the nozzle size, the flow rate and viscosity of the extruded liquid, and the vibrational frequency applied, and can be controlled by selecting the corresponding settings on the encapsulator device *(19)*.

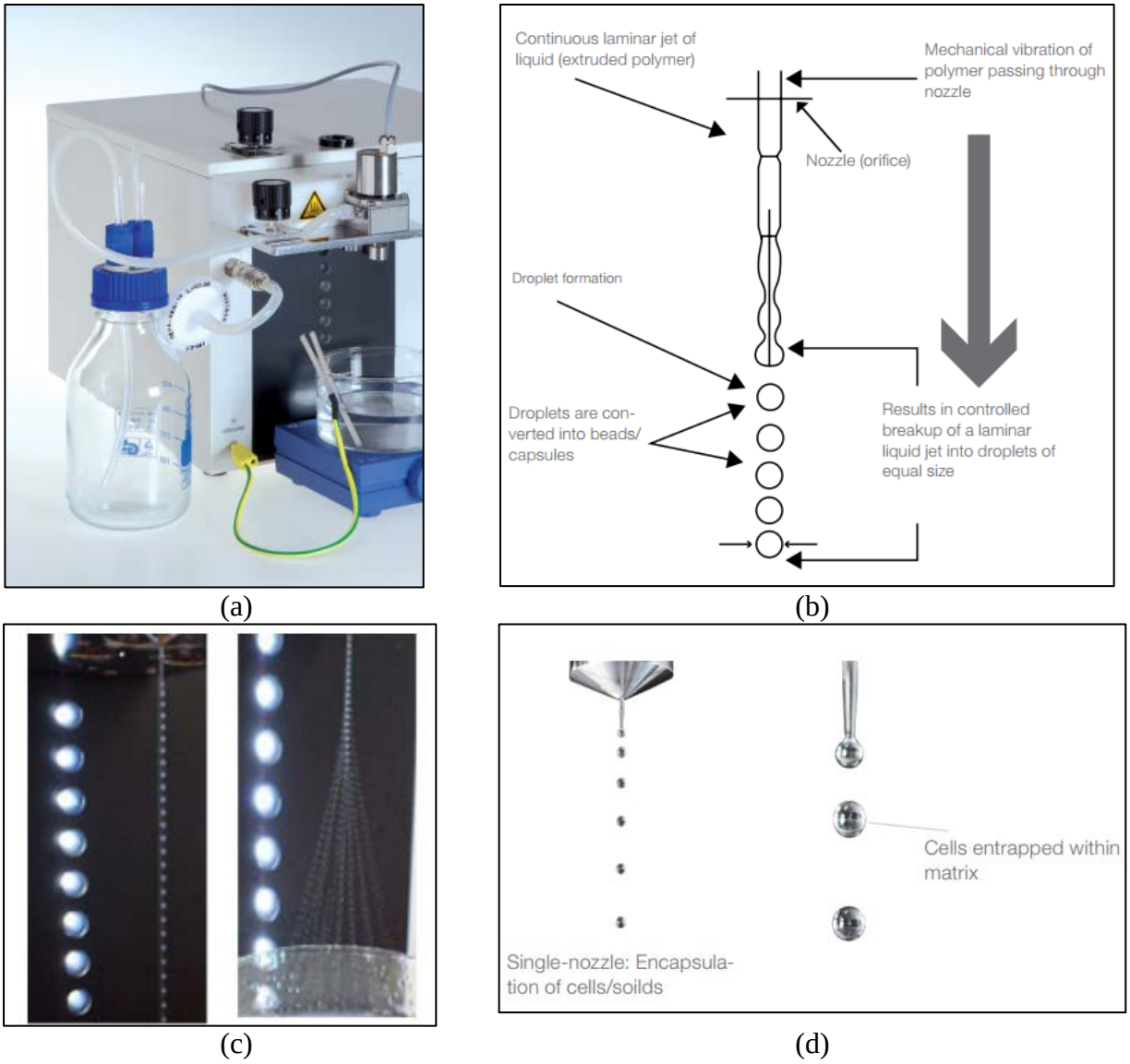

Figure 2. (a) Assembled setup of the BUCHI Encapsulator B-390 for bead production; (b) Schematic display of the operational principle of the BUCHI Encapsulator illustrating the vibrational frequencies for the controlled breakup of a laminar liquid jet into equally sized droplets; (c) Alginate droplet chain produced using set of parameters (left) and dispersion of the droplets using electrostatic charge (right); and (d) Real-time image of droplets being produced on the BUCHI Encapsulator using vibration technology.

Wang et al. *(8)* encapsulated a bacterial spore suspension of *Bacillus sphaericus* (10^9 cells/ml) using synthetic hydrogels. The hydrogels were then added to mortar specimens at concentrations of 2 to 5% by weight of cement, with urea, calcium nitrate, and yeast extract as the nutrients. The results showed that the specimens with hydrogel-encapsulated spores had superior crack-width sealing of up to 0.5 mm (compared to a maximum of 0-0.3 mm crack-width healing in the control) and decreased water permeability by 68% (compared to only by 15-55% decrease in the control). In another study, Wang et al. *(9)* prepared a methacrylate modified alginate-based hydrogel to encapsulate bacterial spores. The synthesized hydrogel was found to be suitable for concrete applications, as it had a positive impact on bacterial viability and concrete strength. In addition,

Seifan et al. demonstrated the entrapment of bacterial cells into calcium alginate has no effect on the $CaCO_3$ morphology formed *(36)*.

3.4. Concrete under Wet-Dry Cycles

The moisture content in concrete is a crucial parameter for shrinkage-related cracking in concrete. Concrete shrinks as the moisture is lost to the environment or due to self-desiccation. The magnitude of strain caused by shrinkage is usually proportional to the amount of moisture lost. As concrete shrinks, a certain amount of tensile stress develops due to restraints from adjunct materials or connected members. The stresses may exceed tensile strength, causing concrete to crack. Among the factors that may lead to moisture content variations in concrete, wet-dry cycles are one of the most aggressive environments suffered by concrete, and the dry-wet regions in concrete are usually regarded as the critical parts pertaining to durability. An experimental study showed that the interior relative humidity of concrete is periodically changed during dry-wet cycles. As concrete undergoes wetting, a fast increase in interior humidity takes place in a short time and then the relative humidity reaches a stable level, which depends on the concrete's strength or on its water-to-cement ratio. On the contrary, as concrete undergoes drying, the interior relative humidity does not drop immediately but decreases gradually. Accordingly, the shrinkage of concrete during dry-wet cycles is also periodically changed, exhibiting shrinkage as drying and expansion as wetting *(37)*.

Wang et al. *(8)* tested specimens that consisted of hydrogel encapsulated *Bacillus sphaericus* spores and nutrients (urea and calcium-nitrate) in mortar specimens. The results showed that after wet-dry cycles of cracked specimens for four weeks involving water immersion for only 1 hour and air-drying in 60% RH for 11 hours, water permeability in all their specimens was decreased. Tziviloglou et al. *(3)* evaluated liquid tightness recovery after cracking and exposure to two different healing regimes: water immersion and wet-dry cycles (each cycle lasted 12 hours) via water permeability tests. The study included a bacteria-based healing agent (*Bacillus* and organic mineral compounds) that was incorporated into lightweight aggregates that were then mixed into mortar specimens. Results showed that the water tightness recovery did not substantially differ either for specimens with or without the healing agent when immersed continuously in water. By contrast, the water tightness recovery increased significantly for specimens containing the healing agent compared to specimens without it, when subjected to wet-dry cycles. Water tightness recovery for specimens with the healing agent exposed to wet-dry cycles reached 76% at 28 days and 98% at 56 days. Cracks for these specimens that were immersed in water for 28 or 56 days clearly exhibited improved crack closure compared to the control subjected to the same healing treatments. Furthermore, cracks of these specimens which were exposed to wet-dry cycles demonstrated complete crack closure in almost all cases. The higher concentration of oxygen in the air during dry cycle seemed to promote the bacterial activity leading to an increased amount of $CaCO_3$ precipitate.

4. METHODOLOGY

4.1. Bacteria Strain Selection

The healing agent selection criteria depended on the bacteria's alkali tolerance and the intended metabolic pathway for the MICP reaction. While the urea hydrolysis pathway is the most commonly studied due to its high biomineralization output, it is important to note that ammonium, a byproduct of this reaction, has detrimental effects in concrete *(22-24)*. For this reason, bacteria species that precipitate calcium carbonate through alternative pathways were preferred. *Bacillus pseudofirmus* and *Diaphorobacter nitroreducens* were both ideal candidates as they have shown promising results in mortar specimens through metabolic conversion of organic acids and denitrification, respectively *(6, 27)*. In addition, both bacterial strains are capable of using oxygen or nitrate as electron acceptors, suggesting they have a higher viability in environments with minimal oxygen availability, provided nitrate is also present within the cementitious matrix. For this reason, the authors proposed testing these bacterial strains in concrete admixed with calcium nitrate, a commercial multi-functional admixture, to help sustain a continuous growth of bacteria that would maintain an active and stable calcite precipitation rate *(11, 27)*.

4.2. Encapsulation of Bacterial Healing Agents

While several techniques were discussed in the literature review, one of the simplest and most effective methods to encapsulate bacteria involved the use of hydrogels, since they can act as a water reservoir to enable or sustain the MICP reaction. Thus, calcium alginate hydrogel beads were used in this study to encapsulate the bacterial cell suspension. The simplest technique for producing alginate beads is extrusion dripping of the healing agent mixture into a calcium chloride gelling bath. The healing agent mixture would be composed of the bacteria cells and nutrients, with a sterilized 1.3% alginate solution. A BUCHI Encapsulator B-390 was used to produce the calcium alginate beads, as shown in Figure 3.

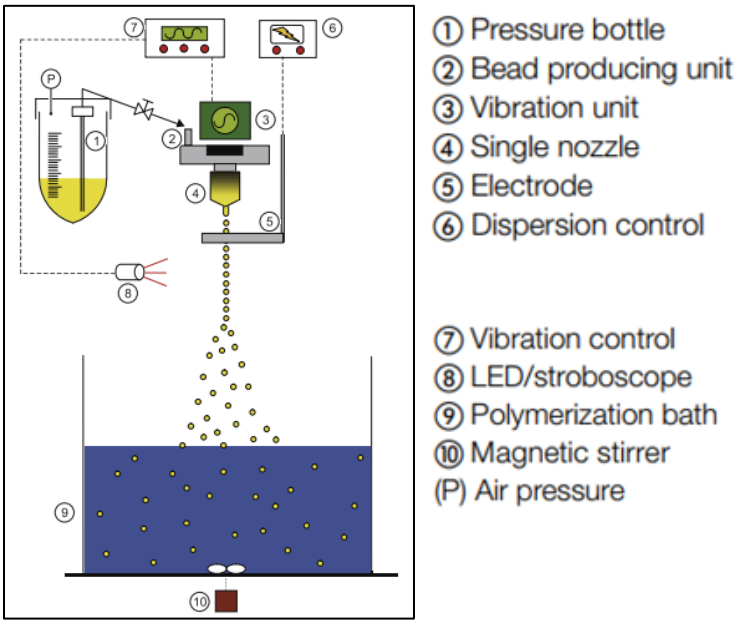

Figure 3. Schematic of the calcium alginate bead preparation using the Encapsulator B-390.

The pressure bottle contained the healing agent mixture, composed of a suspension of either *Bacillus pseudofirmus* or *Diaphorobacter nitroreducens* at 10^7 cells/ml, the 1.3% sodium alginate solution, and 9.64 g/L of magnesium acetate tetrahydrate and 0.48 g/L yeast extract as nutrients. This healing agent mixture was then pumped through a single 450 µm nozzle, which featured a vibration unit that converts a laminar-flow fluid jet into regular-sized droplets. This allows higher production rates without losing control of the droplet size distribution. A magnetic stirrer was used to gently stir the 0.1M calcium chloride gelling bath at an agitation rate of 200 rpm, where the beads were left to cure for 30 minutes. Finally, the beads were rinsed with de-ionized water and recovered with a coarse fritted vacuum filter. The calcium alginate beads' morphology was then characterized with an optical microscope, where at least 250 diameter measurements were taken to evaluate its particle size distribution.

4.3. Concrete Mix Design

The concrete mix design selected for this project resembled a typical mixture used for rigid pavements in Louisiana. A water-cement ratio of 0.48 was selected, with a coarse aggregate to fine aggregate ratio of 60/40. The nominal maximum aggregate size was 19 mm for the coarse aggregate, and 4.76 mm for the fine aggregate, respectively. The calcium alginate beads were embedded at varying concentrations by weight of cement to determine the optimal dosage required for self-healing. Polymer fibers were added to increase the ductility of the concrete specimens that will be cracked or damaged for this study. A superplasticizer was added to increase the workability of the concrete mix. A defoaming agent was also added at a dosage of 0.1% by weight of cement to counter the increases in air voids caused by the addition of capsules in concrete. Lastly, calcium nitrate was added as an admixture at 2% by weight of cement as a supplemental nutrient for the bacterial strains. The details of the concrete mix design are shown in Table 2.

Table 2. Concrete mix design.

Material Description	**Proportions (kg/m^3)**
Aggregate 1: Concrete Sand	729
Aggregate 2: #67 Limestone	1020
Cement: Holcim Type I	297
Water: Mixing water	142
Air (%)	5.0
38 mm Polymer Fibers	5
Admixture 1: Superplasticizer (ml/100 kg)	291
Admixture 2: Calcium alginate beads* (%)	Varied (0%, 0.5%, 1.5%, 3.0%)
Admixture 3: Defoaming agent* (%)	0.1
Admixture 4: Calcium Nitrate* (%)	2.0

4.5. Self-Healing Concrete Testing

The concrete samples were cast and cured in laboratory settings per ASTM C192 guidelines. Fresh concrete properties were measured with slump and air tests per ASTM C143 and ASTM C231, respectively. Table 3 shows characteristics of the specimens used in this study. It is important to note that two different types of control specimens were used in this study. The first control group (Control NC) did not have alginate beads embedded, whereas the second control group (Control 3%C) did have alginate beads with nutrients but no bacteria cells.

Table 3. Specimen group descriptions.

Specimen ID	Bacteria Strain	Concentration (% by weight of cement)
Control NC	N/A	0
Control 3%C	N/A	3.0
DN 0.5%	*Diaphorobacter nitroreducens*	0.5
DN 1.5%	*Diaphorobacter nitroreducens*	1.5
DN 3.0%	*Diaphorobacter nitroreducens*	3.0
B 0.5%	*Bacillus pseudofirmus*	0.5
B 1.5%	*Bacillus pseudofirmus*	1.5
B 3.0%	*Bacillus pseudofirmus*	3.0

A summary and description of variables in the self-healing concrete testing is listed in Table 4.

Table 4. Variables for self-healing concrete testing.

Variables	Content
Bead loading	0%, 0.5%, 1.5%, 3.0%
Bacterial strains	Bacillus Pseudofirmus, Diaphorobacter Nitroreducens
Curing condition	Wet-dry cycles: 8 hrs. water immersion; 16 hrs. drying in 50% relative humidity (RH)
Effect of Capsules on intrinsic concrete properties	Compressive strength (3 cylinders for each loading) Modulus of Elasticity (3 cylinders for each loading)
Self-Healing Evaluation (after 3, 7, 14, and 28 wet-dry cycles)	Stiffness recovery (3 cylinders for each loading) Crack-healing efficiency (3 Beams for each loading)

Six 100 mm x 200 mm concrete cylinders were prepared for compressive strength (ASTM C39), and static modulus of elasticity tests (ASTM C469). After measuring the 28-day modulus of elasticity, the specimens were then subjected to four cyclic loads at 90% of their ultimate strength to induce damage. The modulus of elasticity test was conducted again on all samples to record the degree of damage. In addition, three 150 mm x 150 mm x 280 mm concrete beams were prepared for investigating the crack-sealing efficiency. All beam specimens were subjected to a 3-point loading system, where a displacement rate of 0.125 mm/sec was applied until a crack was induced. Once the damage was measured for both concrete cylinder and beam specimens, the samples were then conditioned in wet/dry cycles consisting of 8 hours of water immersion and 16 hours of air drying at a 50% relative humidity chamber. Modulus of elasticity retests and crack width measurements were made after 3, 7, 14, and 28 wet/dry cycles for the cylinder and beam specimens, respectively. The self-healing concrete testing sequence is illustrated in Figure 4.

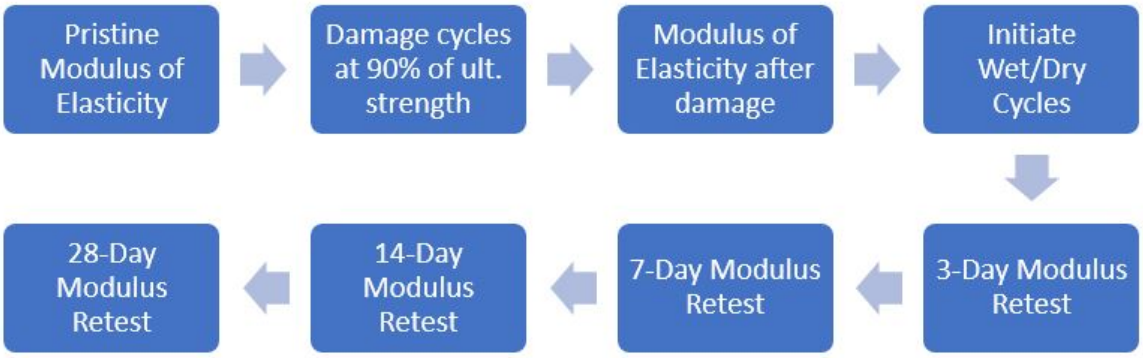

Figure 4. Testing sequence to evaluate self-healing with concrete cylinder.

4.6. Crack-Sealing Quantification

The polymer fibers added ductility to the concrete beams, which enabled the specimen to crack from the bottom of the beam towards three quarters of the beam's side lengths without sudden failure. Both the side cracks and bottom cracks were monitored over time to evaluate concrete's rate of autonomous crack repair, whether it is through concrete's autogenous healing process, or through an enhanced self-healing process aided by MICP. The side cracks generally feature a wide range of crack widths, from hairline cracks extending to larger crack widths at the tension fiber of the beam. This can be favorable for identifying potential crack width limitations, since the bottom cracks feature larger, deeper, and more fairly uniform crack widths which could limit self-healing.

After cracking the beam specimens, the self-healing efficiency was monitored over time with a stereo with a digital camera attached. Figure 5 illustrates the testing schedule used in this study. Crack lengths of 65 mm were observed for each individual beam's side cracks, taking at least 300 measurements per replicate (thus totaling 195 mm of observed side crack length and over 900 measurements for each specimen group). In addition, crack lengths of 25 mm were observed for each individual beam's bottom cracks, taking at least 75 measurements per replicate (thus totaling 75 mm of observed bottom crack length and over 225 measurements for each specimen group). The captured images from each crack were stitched together with Microsoft's Image Composite Editor and the crack widths were measured linearly with the ImageJ processing program. The specimens were then inspected for healing after 3, 7, 14, and 28 wet/dry cycles.

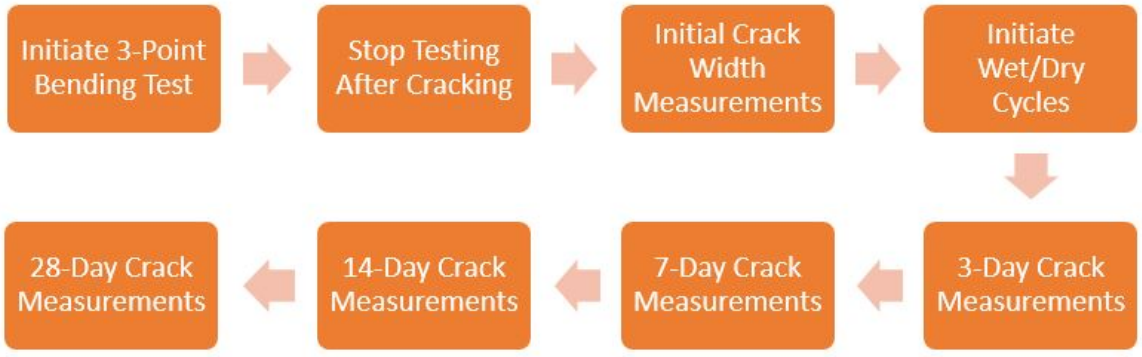

Figure 5. Testing sequence to evaluate self-healing on cracked concrete beams.

4.7. Healing Product Characterization

After 28 wet/dry cycles, the healing products formed at the cracked areas were scraped and sprinkled on a pin stud with double-sided tape. The samples were then sputter coated with platinum for 4 min before they were imaged in the secondary electron mode at an accelerating voltage of 10 kV. Next, energy dispersive spectroscopy (EDS) spectrums were collected under the point analysis and area modes for characterization.

4.8. Surface Resistivity

After 28 wet/dry cycles, surface resistivity tests (per AASHTO T 358) were conducted on all specimen groups. This test is useful as an indication of the concrete's chloride ion permeability. Given that the same concrete mix design was used for all specimens (with the exception of the calcium alginate bead loading), a comparison can be made on the effect of the calcium alginate beads after the concrete cylinders were damaged and allowed to heal.

5. ANALYSIS AND FINDINGS

5.1. Calcium Alginate Bead Characterization

Calcium alginate beads were formed through the extrusion dripping process using a commercial encapsulator (BUCHI B-390), where a 1.3% sodium alginate healing agent mixture was dripped through a 450 µm nozzle. The morphology of the calcium alginate beads was inspected using light microscopy, shown in Figure 6. The beads seem mostly spherical and prone to conglomerate.

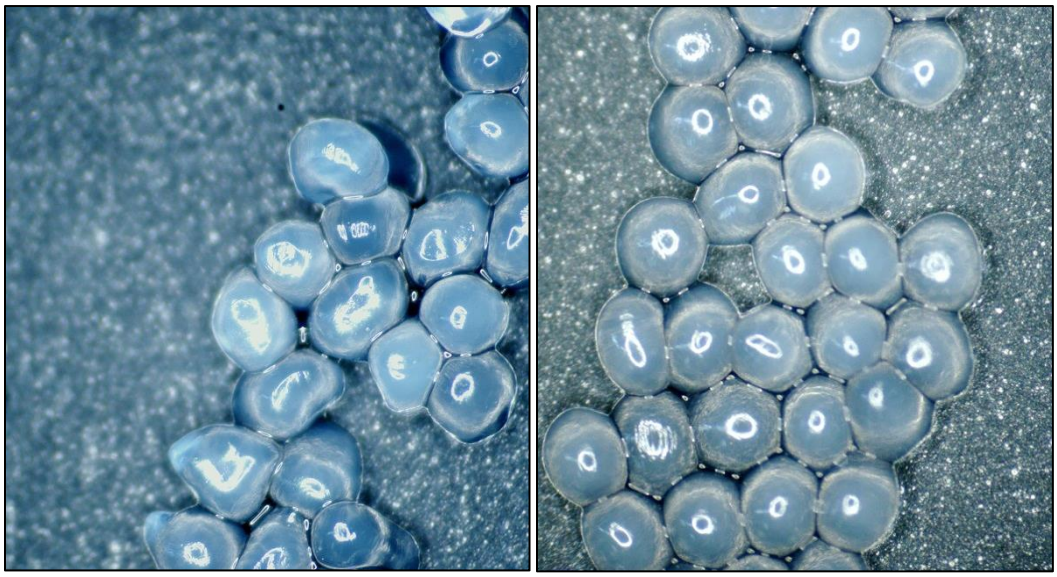

Figure 6. Calcium alginate beads (2X magnification) encapsulating *B. pseudofirmus* (left), and *D. nitroreducens* (right).

The particle size distribution of the diameter of the calcium alginate beads with the microencapsulated bacteria is represented in Figure 7, where at least 300 diameter readings were measured. The mean diameter was 600.75 µm (with a standard deviation of 59.58 µm and a coefficient of variance of 9.92%). The median was 592 µm and the mode was 612 µm. Thus, this shows the encapsulator used was able to control the particle size distribution at satisfactory levels, even though high flow rate was used to produce the beads needed for concrete applications.

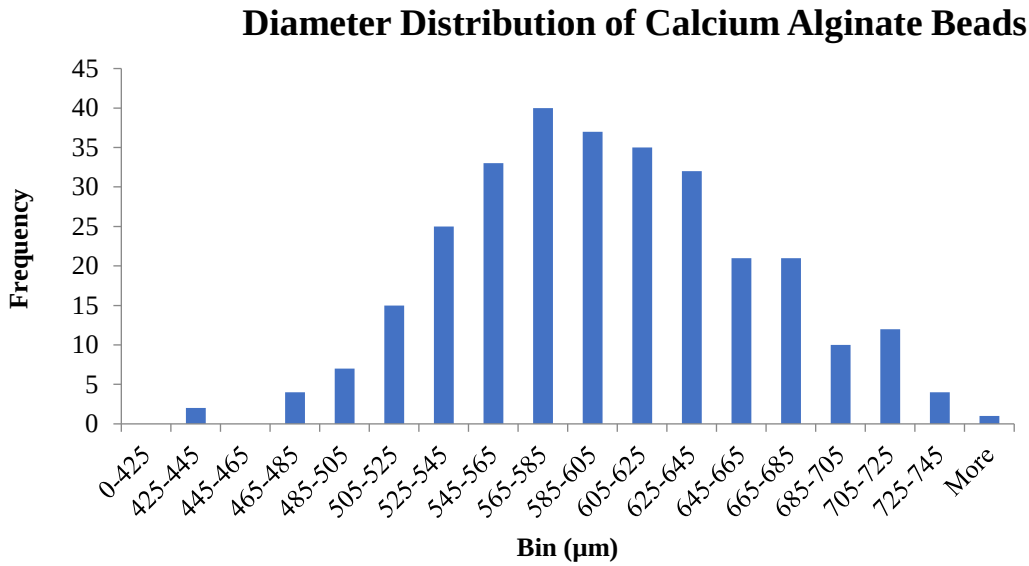

Figure 7. Particle size distribution of the diameter of calcium alginate beads.

5.2. Fresh Concrete Properties

The results from the slump, air entrainment, and unit weight tests are presented in Table 5. Overall, there were minimal differences in the air content between the control groups and the bead-containing specimens. This was attributed to the defoaming agent, which was added in the mix design to control potential increases in air voids caused by the addition of capsules in concrete. Interestingly, as the capsule concentration increased, the air content decreased. This trend differs from what has been studied with polymeric capsules (such as urea-formaldehyde), where larger amounts of capsules yielded higher air contents *(38)*. This difference can be attributed to the encapsulation process, where polymeric capsules require surfactants that tend to increase the air content within the cement paste, while the calcium alginate beads were prepared without surfactants.

Table 5. Fresh concrete properties.

Sample ID	Slump (mm)	Air Content (%)	Unit Weight (kg/m^3)
Control NC	0	3.3	2305
Control 3%C	50	3.1	2275
DN 0.5%	5	3.5	2322
DN 1.5%	0	3.3	2254
DN 3.0%	5	3.2	2319
B 0.5%	0	3.8	2302
B 1.5%	15	3.5	2314
B 3.0%	40	3.1	2304

The concrete mix design was formulated to have a low slump, as this is commonly used for slip form paving applications. In general, a larger amount of calcium alginate beads increased the slump, albeit to a degree where it could still be used for slip form paving (generally ranging from 0-75 mm slumps). There were minimal differences observed in unit weight measurements, indicating that the addition of alginate beads did not seem have a significant effect.

5.3. Compressive Strength

Compressive strength tests were conducted on all specimens per ASTM C39. The results are shown in Figure 8. As expected, a higher concentration of microcapsules yielded weaker compressive strength. This trend that has been observed in numerous studies, since the beads or capsules added in concrete are generally the weakest link within the matrix and do not contribute to strength. However, it is worth noting that the samples with a concentration of 0.5% calcium alginate beads did not have a negative impact on strength, as it was not significantly different than that of the Control NC group.

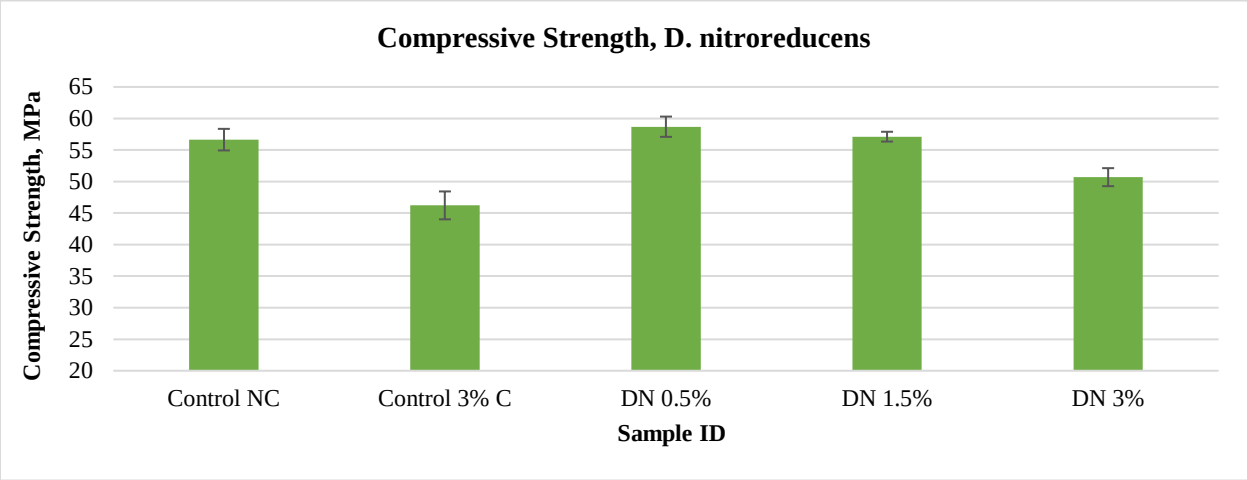

(a)

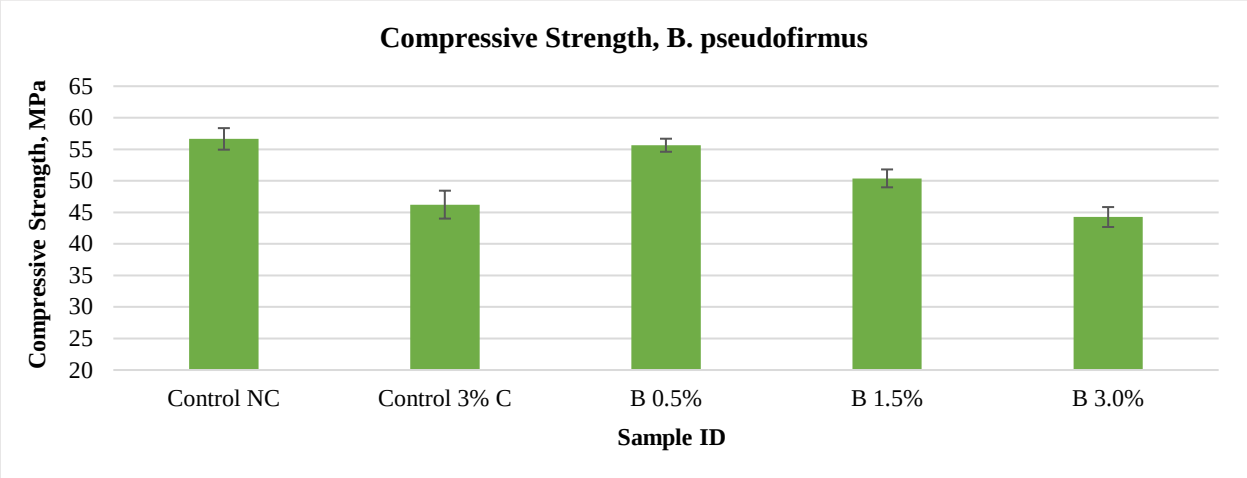

(b)

Figure 8. Compressive strength results for the (a) *D. nitroreducens* specimen groups; (b) *B. pseudofirmus* specimen groups.

A statistical analysis using Fisher's LSD test at a 5% significant level was used to evaluate the effect of alginate bead concentrations with respect to the compressive strength values of all undamaged specimens, as shown in Figure 9. The results show that cylinder specimens with 0.5% calcium alginate beads as well as 1.5% *D. nitroreducens* specimen were not significantly weaker than the Control NC (with no beads). The other specimens (1.5% and 3% *B. pseudofirmus*, the 3% *D. nitroreducens*, and Control 3% C which contains 3% beads with nutrients only) were

significantly weaker than the Control NC. In addition, the 3% *B. pseudofirmus* specimen was not significantly different in compressive strength than the Control 3% C, where both these specimens were the weakest among all groups. Yet, the 3% *D. nitroreducens* specimen was significantly different than the Control 3%C group. This is likely due to the variability of how the capsules are spread within the cementitious matrix.

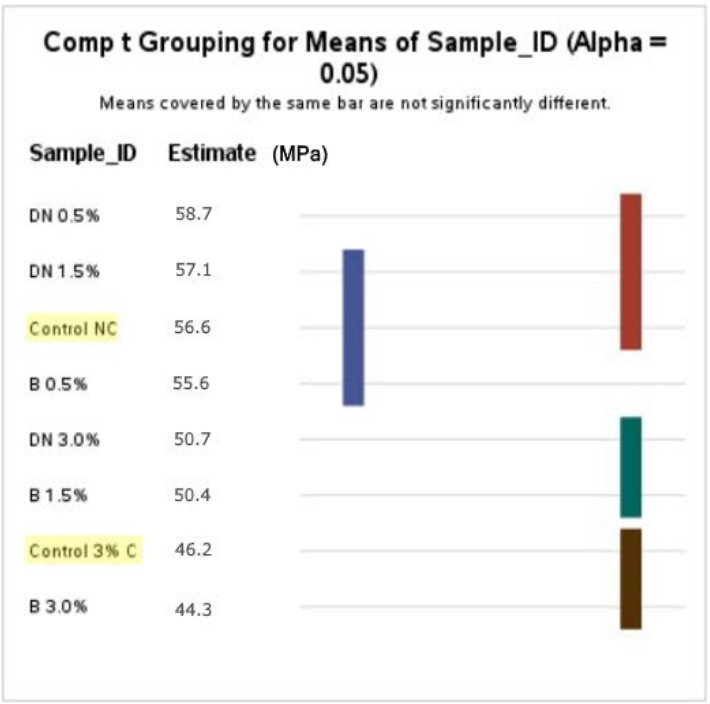

Figure 9. Fisher's LSD test results for the compressive strength (MPa) of the undamaged concrete cylinder specimens.

5.4. Modulus of Elasticity

5.4.1. Pristine Specimens

The static modulus of elasticity was measured for all specimen groups per ASTM C469, illustrated in Figure 10, where the error bars show the standard deviations. The results showed that low alginate bead concentrations of 0.5% to 1.5% (by weight of cement) did not have detrimental effects on the modulus of elasticity, which is highly desired for implementation purposes. These trends were observed for both the *D. nitroreducens* and the *B. pseudofirmus* specimen groups.

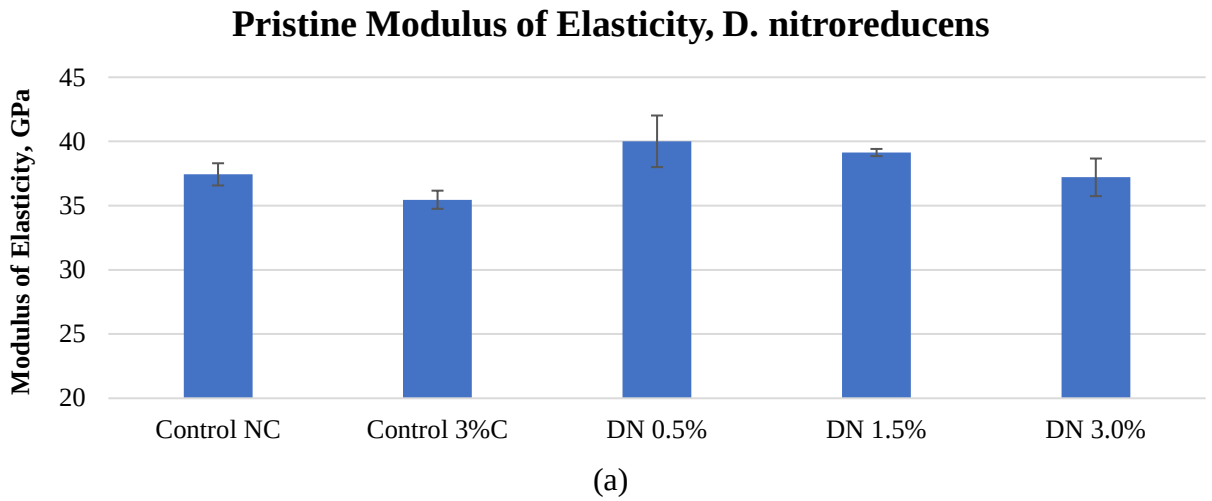

(a)

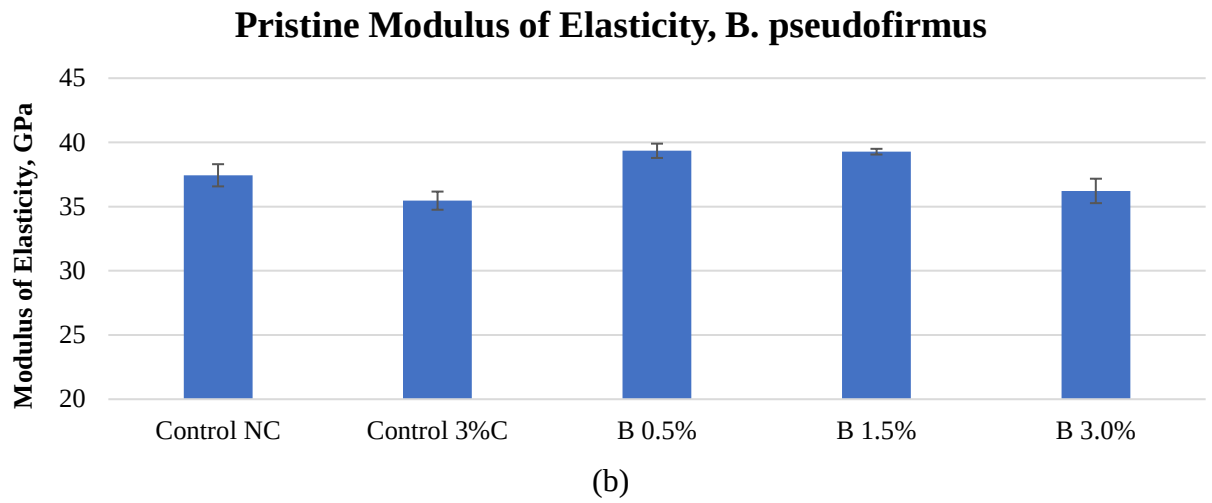

(b)

Figure 10. Modulus of elasticity results for the (a) D. nitroreducens specimen group; (b) B. pseudofirmus specimen group.

A statistical analysis applying Fisher's LSD test at a 5% significance level was used to evaluate the effect of alginate bead concentrations with respect to the pristine modulus of elasticity values as shown in Figure 11. The results showed that the modulus of elasticity was significantly higher for all specimens containing calcium alginate beads at 0.5% and 1.5% than both the control specimens. Remarkably, a high calcium alginate bead concentration of 3% did not yield significant differences between the modulus of elasticity values of both the control specimens.

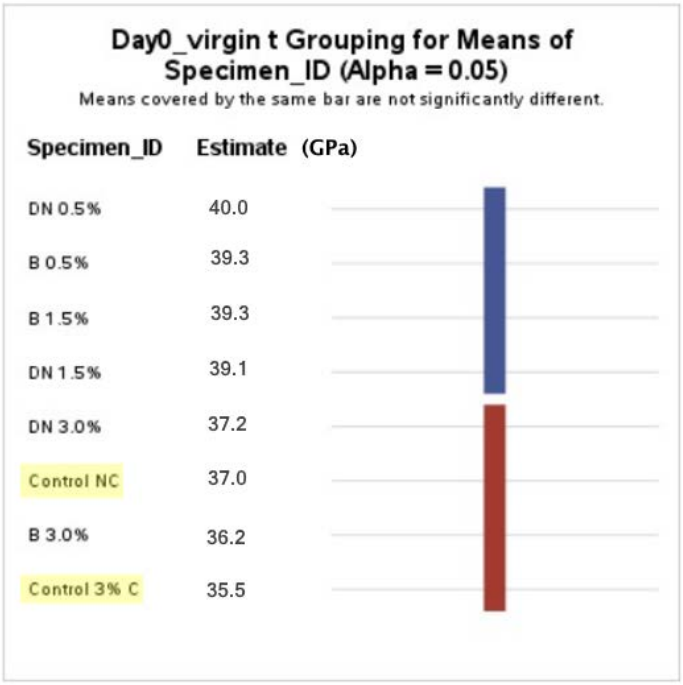

Figure 11. Fisher's LSD test results for the pristine modulus of elasticity (GPa) of the cylinder specimens on day 0.

5.4.2. Stiffness Recovery

After the pristine modulus of elasticity was measured, all specimen groups were then damaged through uniaxial compression consisting of four load cycles up to 90% of their ultimate strength. The modulus of elasticity after damage was then measured, before the healing regime of wet/dry cycles (8 hours water immersion; 16 hours of air drying at 50% RH) began. Retests of modulus of elasticity were then conducted to measure the stiffness recovery over time, illustrated in Figure 12.

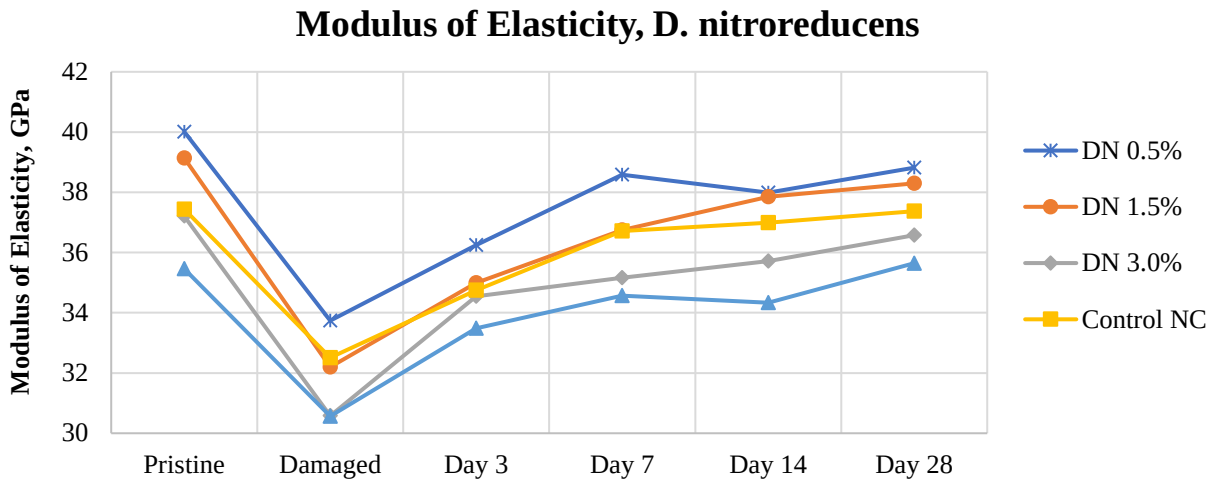

(a)

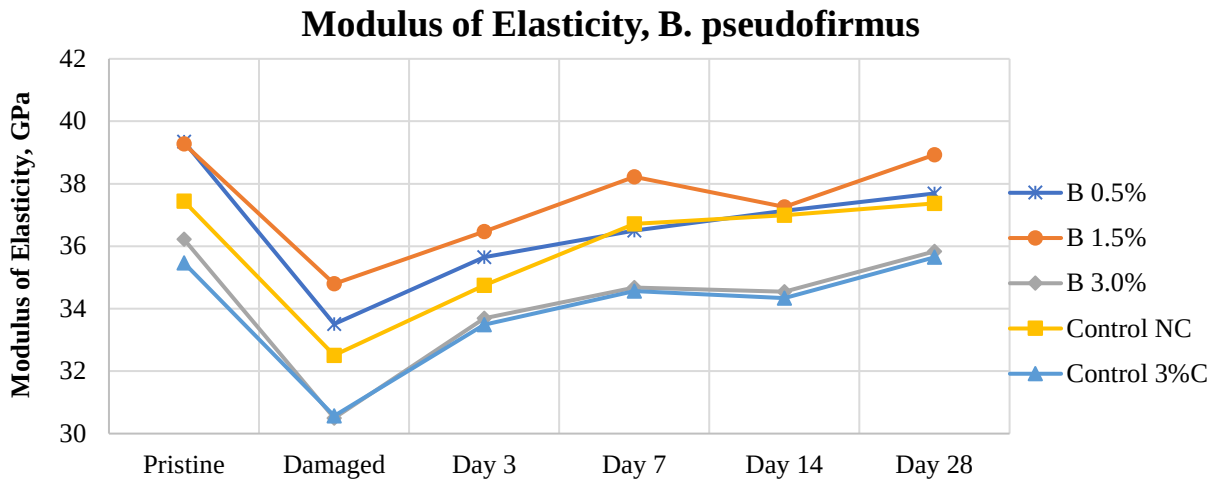

(b)

Figure 12. Modulus of elasticity test results over time of (a) *D. nitroreducens* specimen groups; (b) *B. pseudofirmus* specimen groups.

Overall, exposure of wet/dry cycles resulted in a stiffness recovery over time for all specimens. This can be attributed to the intrinsic, autogenous healing capability of concrete when exposed to moisture. However, to evaluate whether the bacterial healing agent enhanced the stiffness recovery, it was important to normalize the results obtained over time. This was expressed as the percentage increase in modulus relative to the damage stage, shown in the formula below.

$$SR = \frac{M_{dmg} - M_{day}}{M_{dmg}} \times 100 \qquad [1]$$

where:
SR = Stiffness recovery (%);
M_{dmg} = Modulus of elasticity (GPa) for damaged cylinder sample; and
M_{day} = Modulus of elasticity (GPa) for cylinder sample on day of analysis (day 3, 7, 14, or 28).

The stiffness recovery for all specimens was then plotted on Figure 13. It can be observed that those specimens with the highest calcium alginate concentrations resulted in higher increases in stiffness recovery. Interestingly, this observation also applies with the control specimens embedded with 3% calcium alginate beads without bacteria. This could be attributed to the calcium alginate hydrogels acting as a water reservoir that could further the autogenous healing reaction even when the samples are left to air dry.

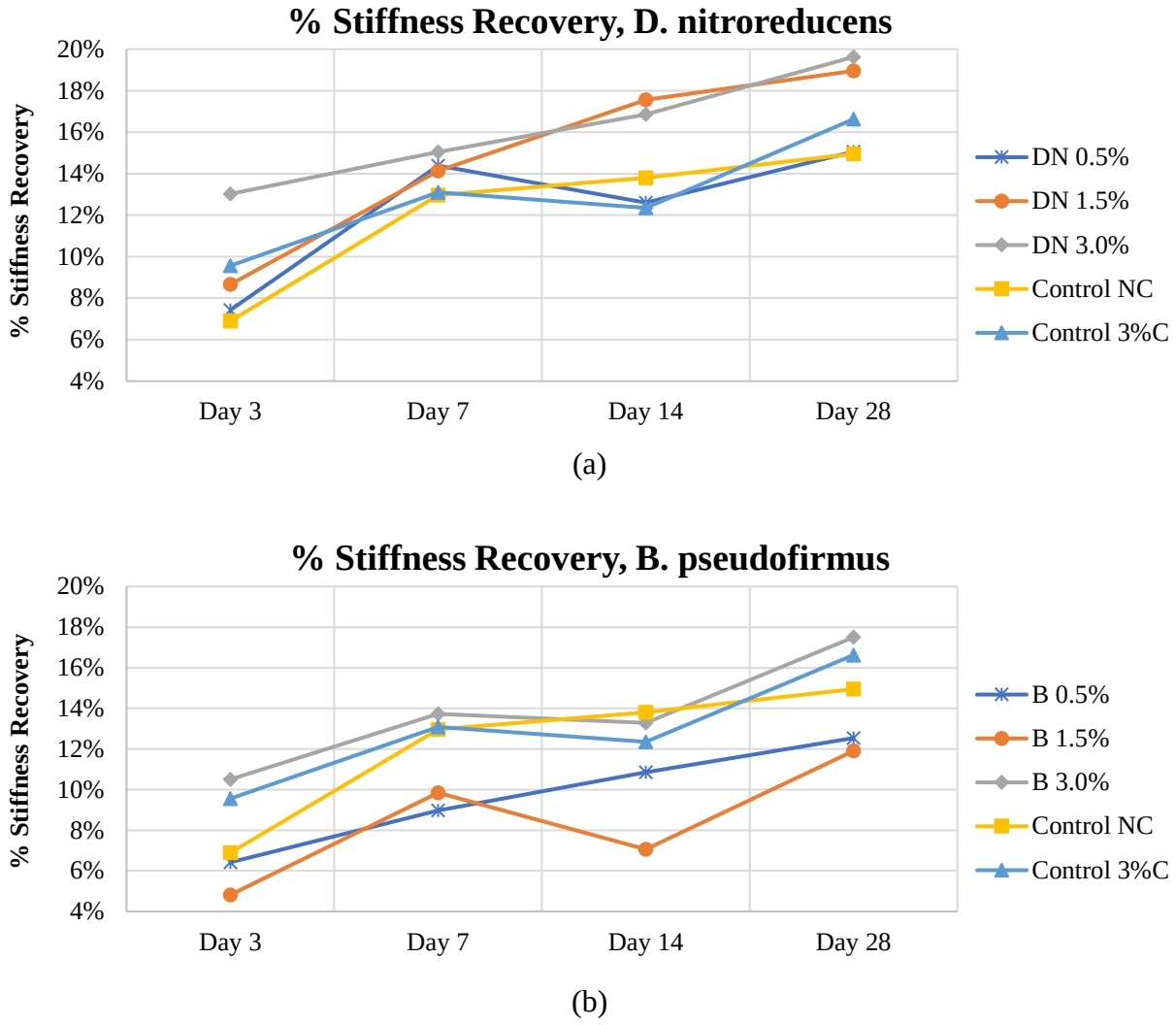

Figure 13. Stiffness recovery over time observed on the (a) *D. nitroreducens* specimen groups; (b) *B. pseudofirmus* specimen groups.

To understand the significance of these results, a statistical analysis using Fisher's LSD test was used to evaluate the effect of the calcium alginate beads (with and without the bio-healing agents) with respect to the stiffness recovery over time (Figure 14). After 3 wet/dry cycles, only the DN 3.0% specimen group exhibited a higher stiffness recovery than the Control NC group. However, the Control 3%C group was not found to be significantly different from the rest of the specimens containing alginate beads, with the exception of B 1.5%. After 7 wet/dry cycles, all specimen groups with bacteria were not significantly different from Control NC and Control 3%C. However, as the wet/dry cycles continue, DN 1.5% has a significantly higher stiffness recovery than Control NC, while Control 3%C is only significantly higher than specimen B 1.5%.

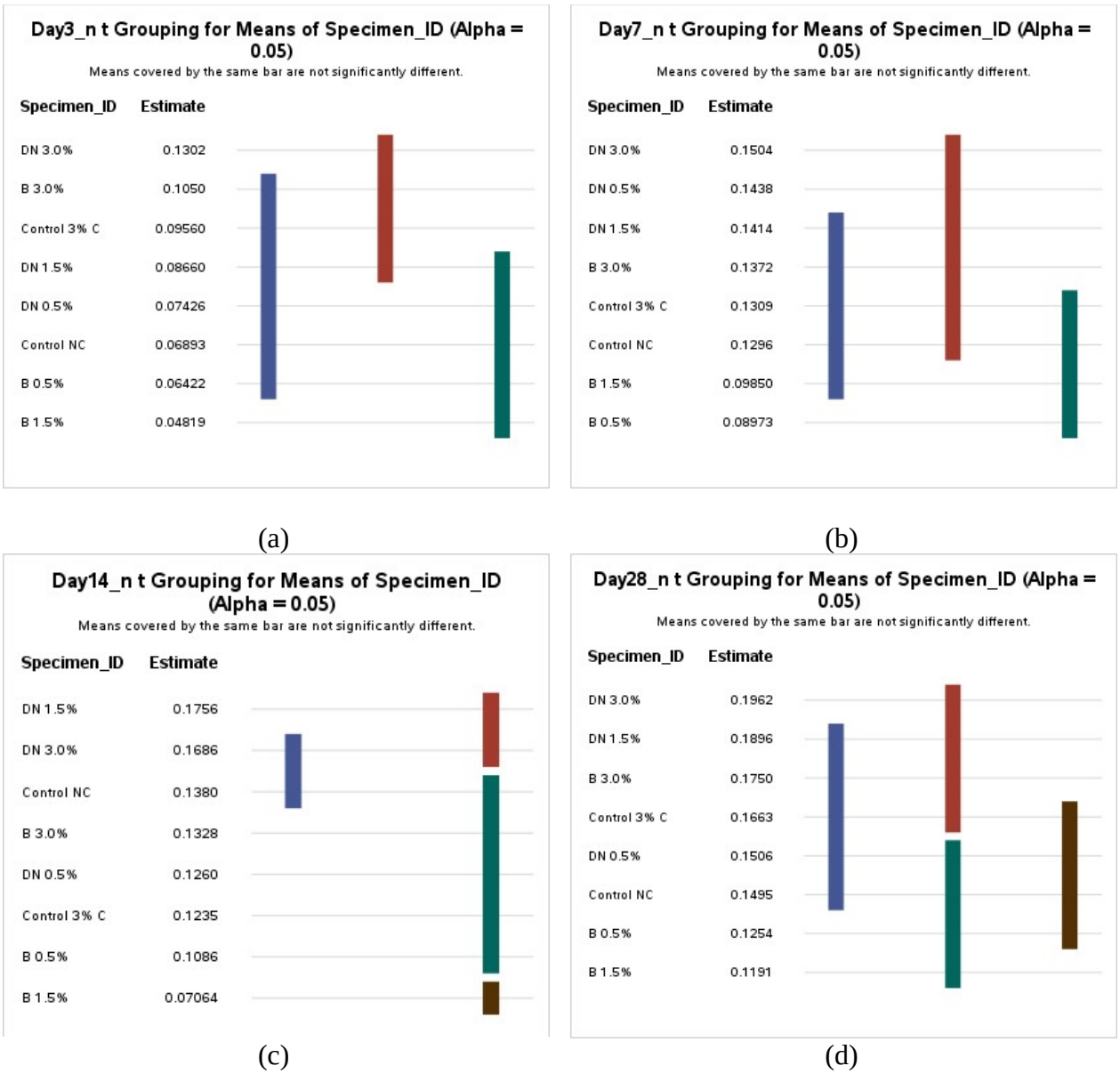

Figure 14. Fisher's LSD results for the normalized stiffness recovery (% difference/100) of the cylinder specimens on (a) day 3; (b) day 7; (c) day 14; and (d) day 28 of the wet/dry cycles.

Overall, these findings indicate that the addition of calcium alginate beads with bacteria do not necessarily yield a higher stiffness recovery than the reference specimens. This can be attributed to the fact that there were no surface cracks formed when damaging the cylinders (rather, internal micro-cracks at such loading constraints). As such it is possible that not enough alginate beads were ruptured, or not enough oxygen (or calcium nitrate) was available to the bacteria nearby to initiate the MICP reaction. Alternatively, in the event that the MICP reaction occurred successfully in such conditions, it is possible that the calcium carbonate healing products formed did not contribute to a significantly higher stiffness recovery than the reference specimens. Future research may be needed to establish the degree of healing within the internal micro-cracks formed from overloaded concrete cylinders. In addition, while there were discrepancies in performance were

observed between the *B. pseudofirmus* and *D. nitroreducens* specimen groups at equivalent dosages, in the majority of cases these differences were not statistically significant.

5.5. Crack-Sealing Efficiency

After subjecting the cracked beams to wet/dry cycles, the specimens were monitored periodically to evaluate the healing efficiency. The healing product appeared to be of crystalline nature, indicating there could be calcium carbonate and possibly calcium hydroxide present. Images comparing the initial cracks and after 28 wet/dry cycles are shown in Figure 15. The Control NC specimens also showed crack-sealing, which can be attributed to the autogenous healing capability of concrete exposed to moisture.

(a) Control, No Capsules (Day 0)

(a) Control, No Capsules (Day 28)

(b) Control, 3% Capsules (Day 0)

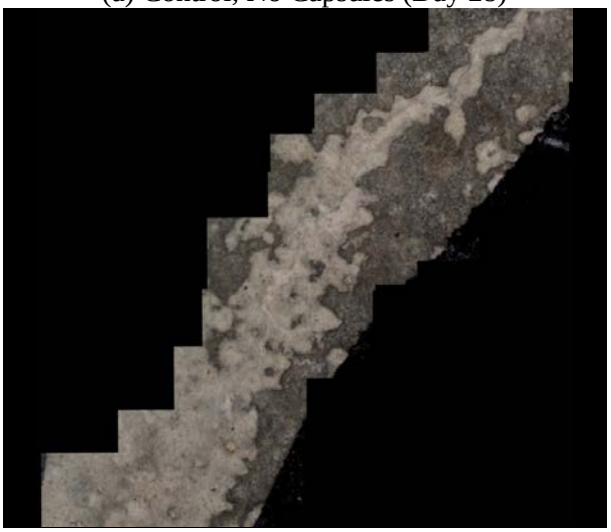

(b) Control, 3% Capsules (Day 28)

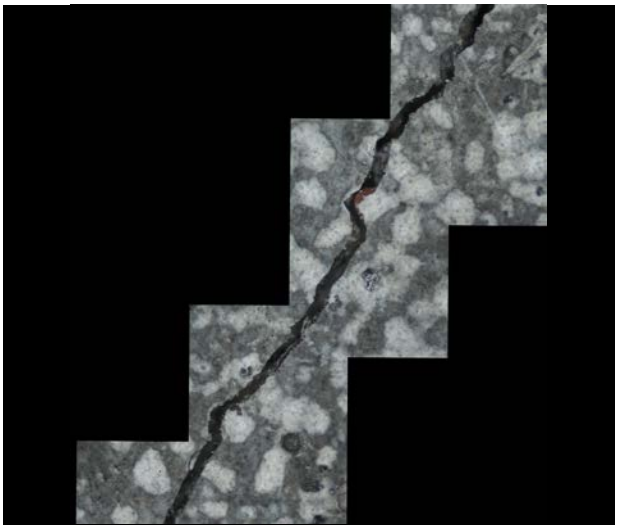

(c) *D. nitroreducens* 0.5% (Day 0)

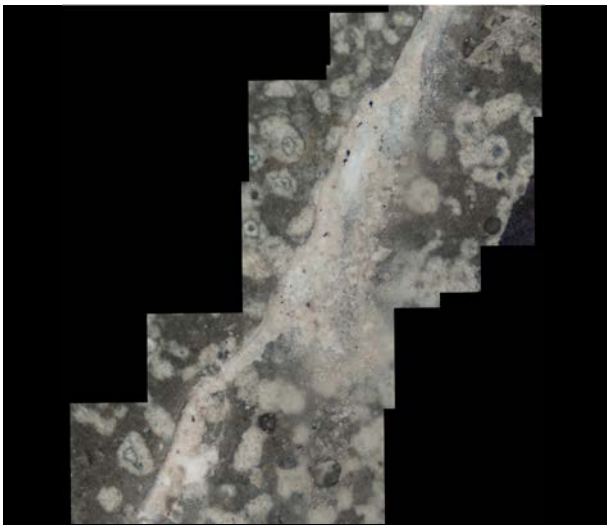

(c) *D. nitroreducens* 0.5% (Day 28)

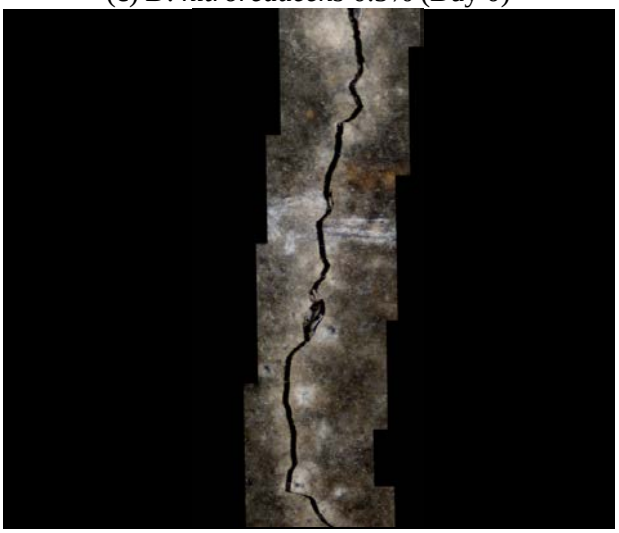

(d) *D. nitroreducens* 1.5% (Day 0)

(d) *D. nitroreducens* 1.5% (Day 28)

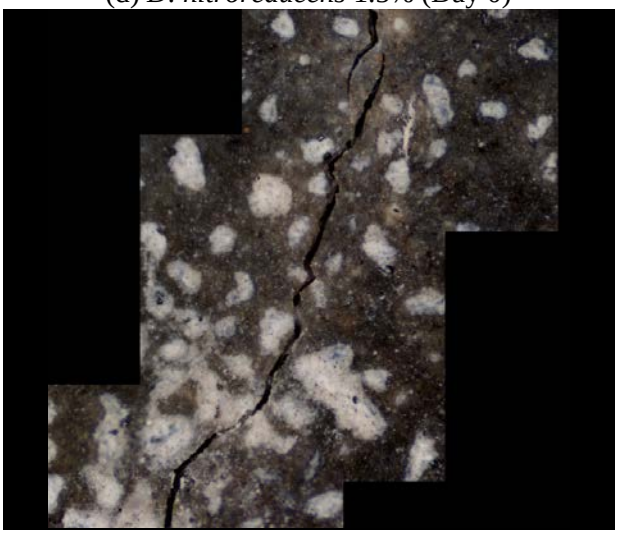

(e) *D. nitroreducens* 3.0% (Day 0)

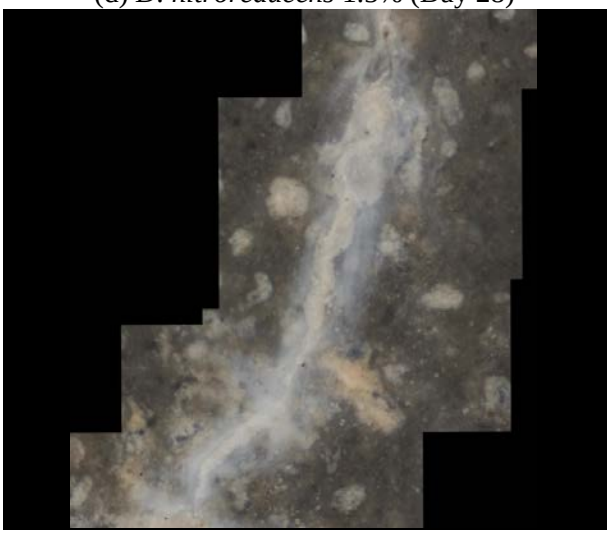

(e) *D. nitroreducens* 3.0% (Day 28)

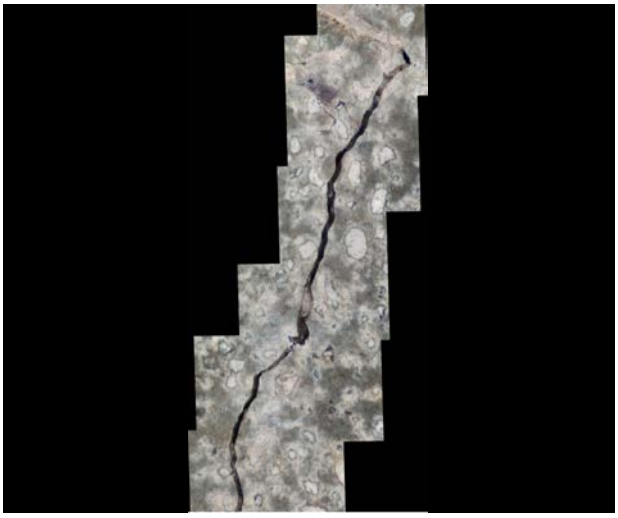

(f) *Bacillus pseudofirmus* 0.5% (Day 0)

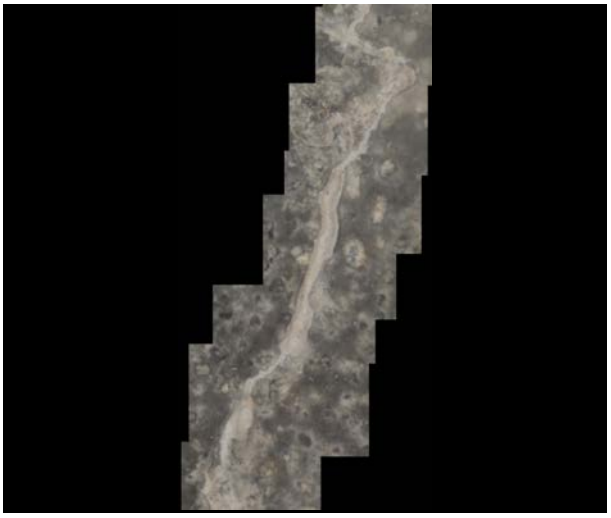

(f) *Bacillus pseudofirmus* 0.5% (Day 28)

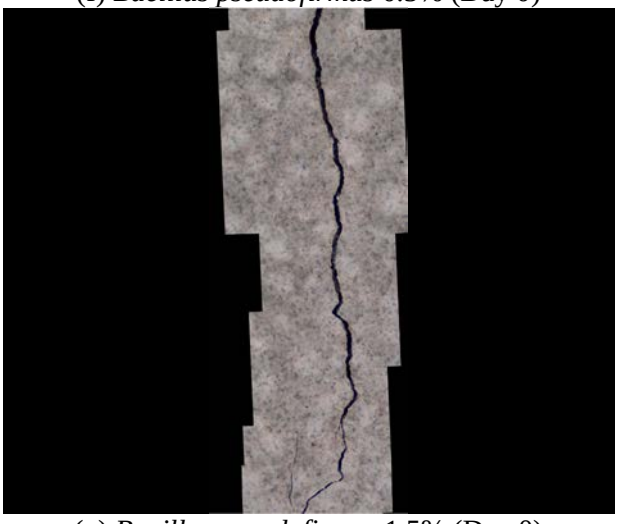

(g) *Bacillus pseudofirmus* 1.5% (Day 0)

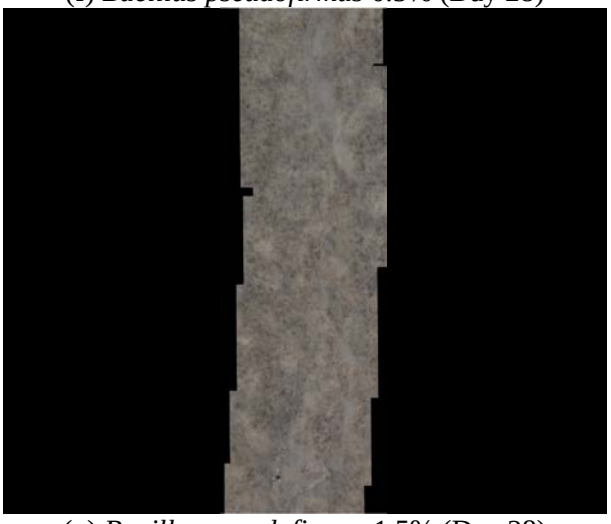

(g) *Bacillus pseudofirmus* 1.5% (Day 28)

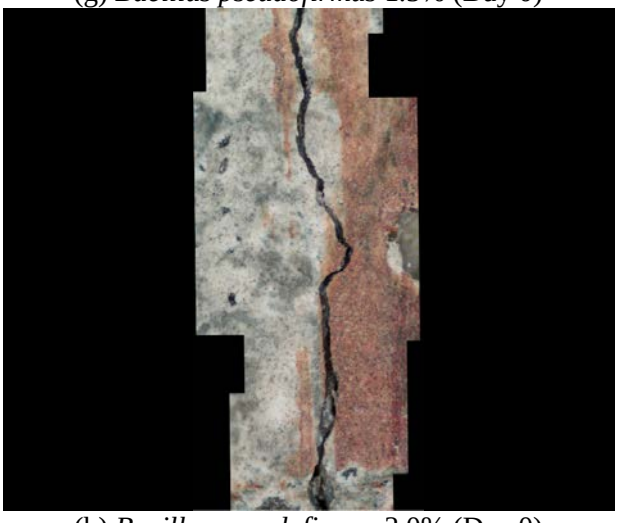

(h) *Bacillus pseudofirmus* 3.0% (Day 0)

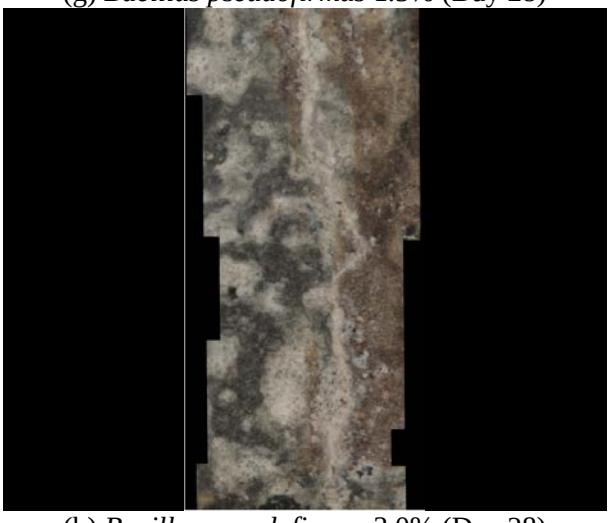

(h) *Bacillus pseudofirmus* 3.0% (Day 28)

Figure 15. Image comparison of side cracks at Day 0 and Day 28, respectively, for samples (a) Control NC; (b) Control 3%C; (c) DN 0.5%; (d) DN 1.5%; (e) DN 3.0%; (f) B 0.5%; (g) B 1.5%; (h) B 3.0%.

For a quantitative assessment, at least 900 measurements were obtained per specimen group from the side cracks that covered a variety of crack widths, and at least 225 measurements were obtained from the bottom cracks per specimen group. The average crack widths (CW) measured and their respective standard deviations (SD) were reported in Table 6 and Table 7 for the side cracks and bottom cracks, respectively. In general, it can be observed that the side cracks showed healing at a significantly larger rate than the bottom cracks. This can be attributed to the large crack widths measured at the bottom cracks, since it is a known that larger crack widths can limit the healing efficiency.

Table 6. Mean crack widths measured from side cracks.

	Day 0		Day 3		Day 7		Day 14		Day 28	
Sample ID	CW (μm)	SD	CW (μm)	SD	CW (μm)	SD	CW (μm)	SD	CW (μm)	SD
Control NC	174	39	160	49	125	50	115	47	113	45
Control 3%C	120	21	75	30	55	17	43	15	39	16
DN 0.5%	150	14	101	19	78	15	61	10	60	10
DN 1.5%	143	28	92	17	75	19	67	18	65	18
DN 3.0%	171	69	114	60	92	58	80	51	78	51
B 0.5%	135	29	102	15	75	11	63	13	60	12
B 1.5%	121	23	93	22	79	13	77	16	73	15
B 3.0%	127	17	79	18	69	21	59	25	57	26

Table 7. Mean crack widths measured from bottom cracks.

	Day 0		Day 3		Day 7		Day 14		Day 28	
Sample ID	CW (μm)	SD	CW (μm)	SD	CW (μm)	SD	CW (μm)	SD	CW (μm)	SD
Control NC	342	36	335	41	326	37	322	38	315	39
Control 3%C	276	70	271	70	270	70	269	69	267	69
DN 0.5%	372	119	357	126	355	125	354	123	352	123
DN 1.5%	313	4	301	14	298	12	297	11	296	12
DN 3.0%	362	120	344	100	332	81	330	80	328	80
B 0.5%	275	74	267	68	264	68	262	68	261	68
B 1.5%	253	66	238	70	237	70	236	70	236	70
B 3.0%	250	28	247	30	245	31	244	31	244	32

Tables 6 and 7 give perspective on the range of crack widths observed after damage, and their potential influence in healing efficiency (given that large crack widths can limit self-healing). While it is challenging to achieve a uniform crack width through a 3-point bending test for all specimen groups, it is evident that the polymer fiber reinforcement added sufficient ductility and crack width control, where the range of crack widths observed after damage did not differ more than 55 microns for side cracks, and 122 microns for the bottom cracks

Given that each specimen has its unique set of crack sizes, the results were normalized by calculating the healing efficiency using the formula below:

$$H_e = \left(\frac{W_i - W_t}{W_i}\right) \times 100 \qquad [2]$$

where:
H_e = Healing efficiency (%);
w_i = Initial crack width (µm); and
w_t = Crack width (µm) at time *t* (day) of analysis (day 3, 7, 14, or 28).

Figure 16 shows the healing efficiencies of the monitored side cracks after 3, 7, 14, and 28 of the wet/dry cycles. As expected, the healing efficiency increased over time for all specimens. From the side cracks, it is worth noting that the lowest healing efficiencies were observed for the Control NC specimens, suggesting that the calcium alginate beads did have an impact in self-healing.

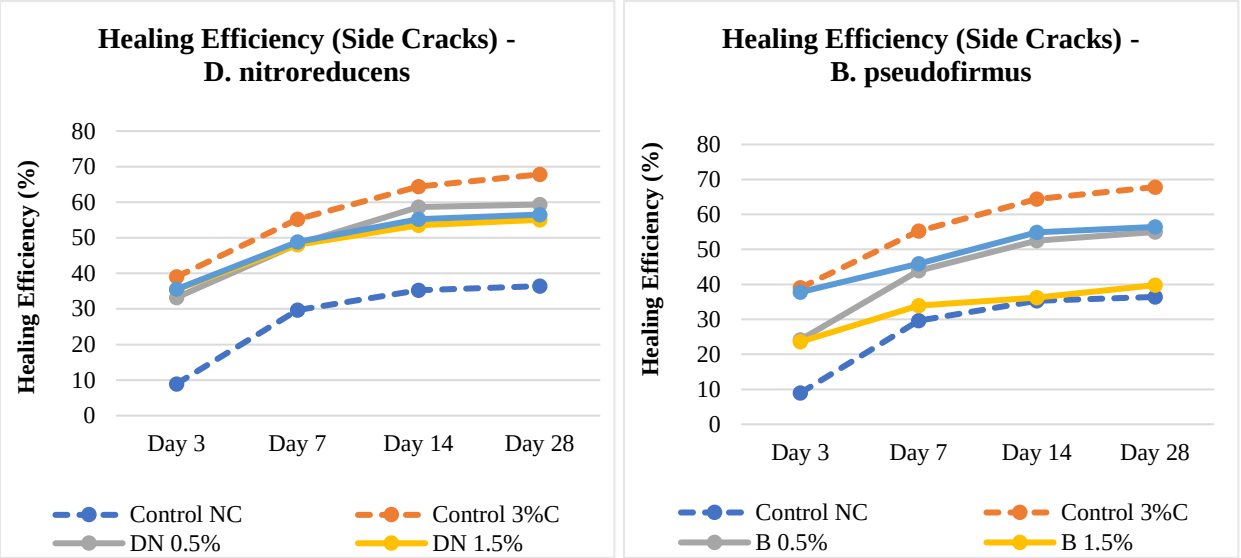

Figure 16. Healing efficiency of the side cracks from the (a) *D. nitroreducens* specimen groups; (b) *B. pseudofirmus* specimen groups.

Fisher's Least Significant Difference (LSD) test was used to analyze the effect of encapsulated bacteria and concentration with respect to the healing efficiencies of the side cracks for all specimen groups, illustrated in Figure 17. For the side cracks, after 3 wet/dry cycles, all specimen groups showed significantly higher healing efficiencies than the Control NC specimens. However, as the number of wet/dry cycles increased over time, in particular at days 14 and 28, all specimens with the exception of DN 1.5%, B 0.5%, and B 1.5% were not significantly different than the Control NC specimens. This indicates that a higher concentration of alginate beads is needed to observe significantly higher healing efficiencies.

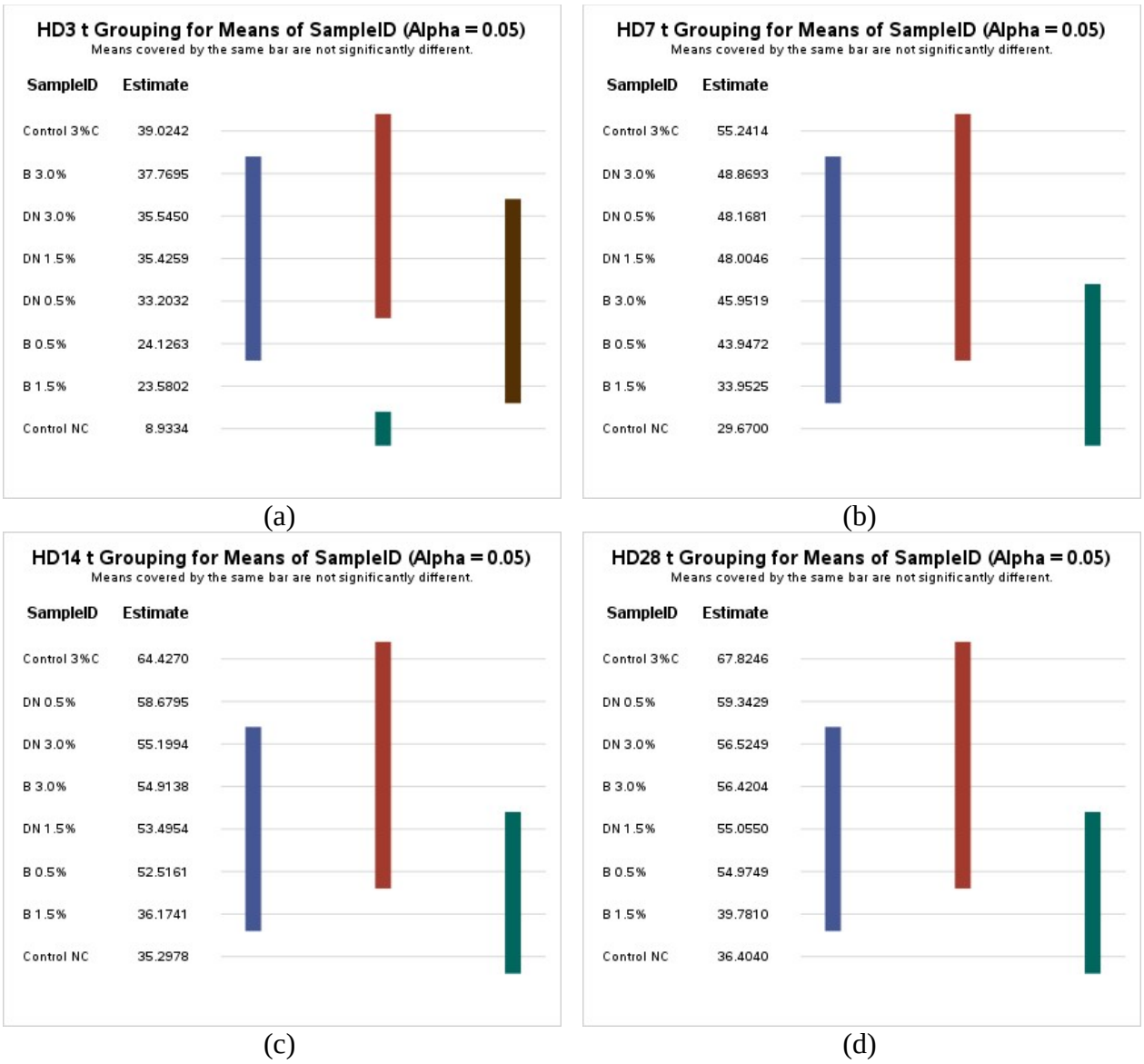

Figure 17. Fisher's LSD results for the normalized crack-healing efficiencies (%) of the side cracks on (a) day 3, (b) day 7, (c) day 14, and (d) day 28 of the wet dry cycle.

It is also worth noting that the Control 3%C specimens also exhibited high healing efficiencies, which can be attributed to the hydrogel's capability to act as a reservoir that further enhances the autogenous healing of concrete. Further research is needed to identify the factors that inhibited stronger healing efficiencies from the specimens containing bacteria, whether it relates to the curing regime or the nutrient selection, or whether an alternative encapsulation mechanism would yield better results. Surprisingly, only specimen group B 1.5% had significantly lower healing efficiencies than the rest of the samples containing alginate beads. This may be an anomaly caused by an improper dispersion of alginate beads within the cementitious matrix.

Besides the side cracks' healing efficiency, the mean crack width reduction was also used as an indication of the degree of self-healing observed in each specimen group, shown in Figure 18. As expected, the mean crack width reduction increased over time for all specimen groups. With the exception of specimen group B 1.5%, all samples containing alginate beads exhibited higher crack

width reductions. The largest crack width reductions were observed on samples DN 3.0% and DN 0.5%, both of which surpassed the reference specimens (Control NC and Control 3%C). Thus, this suggests that some specimens containing bacteria were able to seal larger cracks than the control specimens.

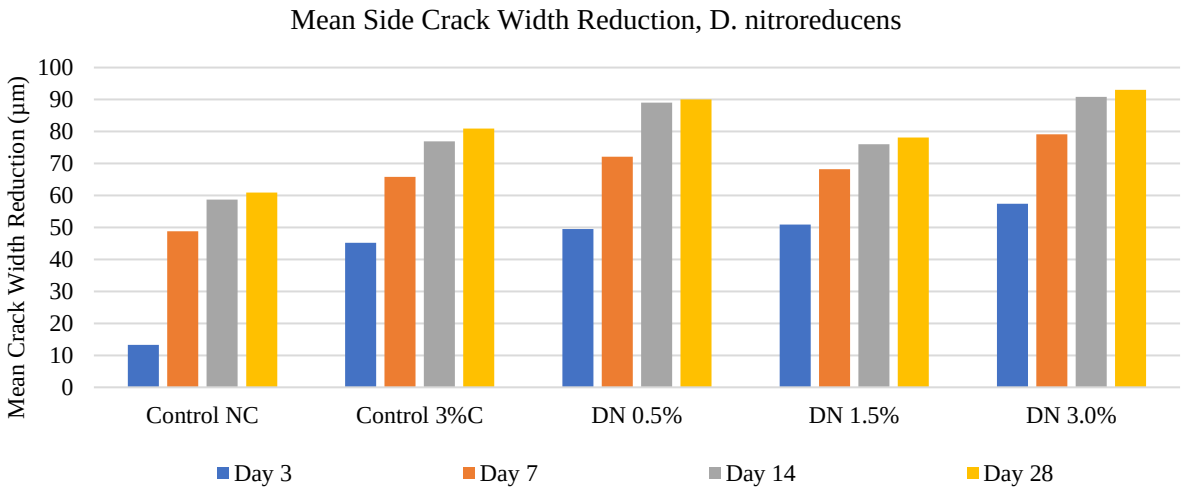

(a)

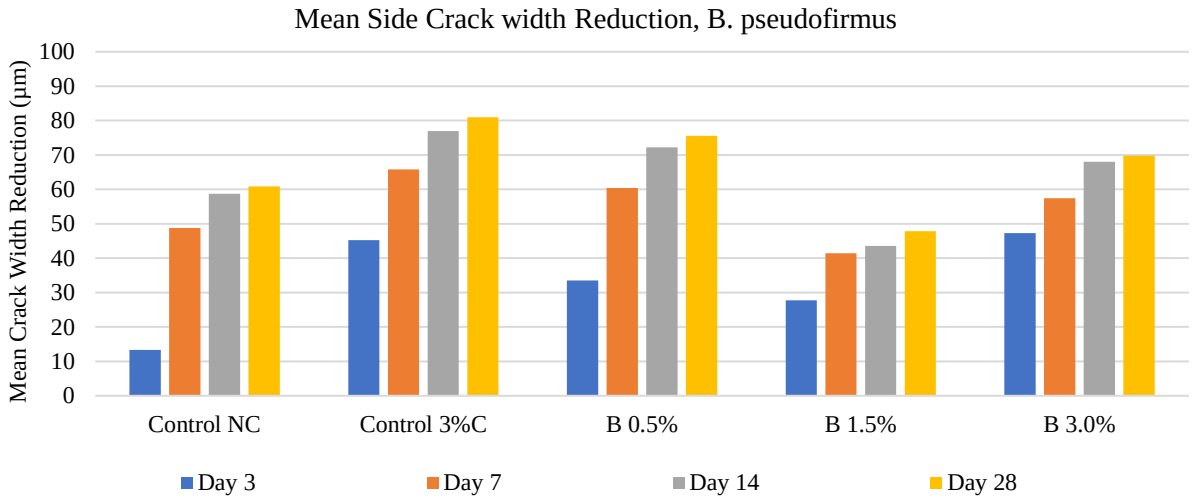

(b)

Figure 18. Mean side crack width reduction over time from (a) *D. nitroreducens* specimen groups; (b) *B. pseudofirmus* specimen groups.

In contrast, the bottom cracks featured minimal healing throughout the 28 wet-dry cycles, as shown in Figure 19. While the mean size of the cracks did decrease over time, the maximum healing efficiency stayed under 8 percent, as opposed to the side cracks which had a healing efficiency up to 68 percent. Indeed, the healing efficiency trends observed from the side cracks did not apply at the bottom cracks. In addition, one of the lowest healing efficiencies at the bottom cracks was observed in Control 3%C, contrasting the favorable results from the side cracks' self-healing.

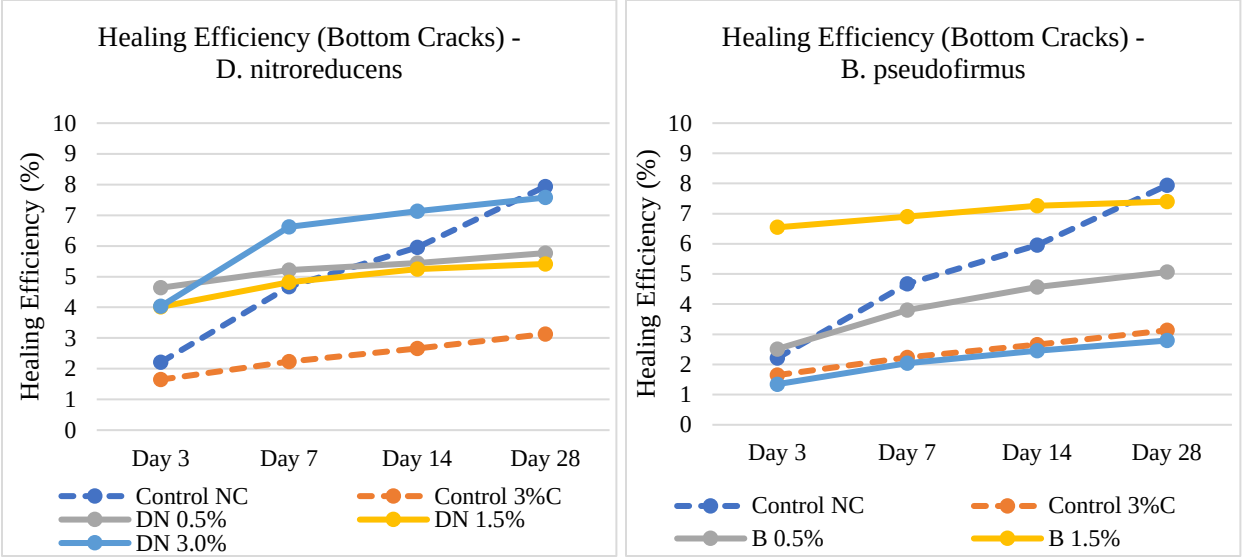

Figure 19. Healing efficiency of the bottom cracks from the (a) *D. nitroreducens* specimen groups; (b) *B. pseudofirmus* specimen groups.

Fisher's LSD was used to analyze the effect of encapsulated bacteria and concentration with respect to the healing efficiencies of the bottom cracks for all specimen groups, shown in Figure 20. The results showed there were no significant differences in the healing efficiencies from the bottom cracks between all specimens. This means that while the healing percentage increased slightly with curing time, the role of bacteria or alginate beads had no appreciable effect on healing the bottom cracks. This may be due to the larger cracks that limited healing at the bottom cracks, as opposed to the narrower and shallower side cracks.

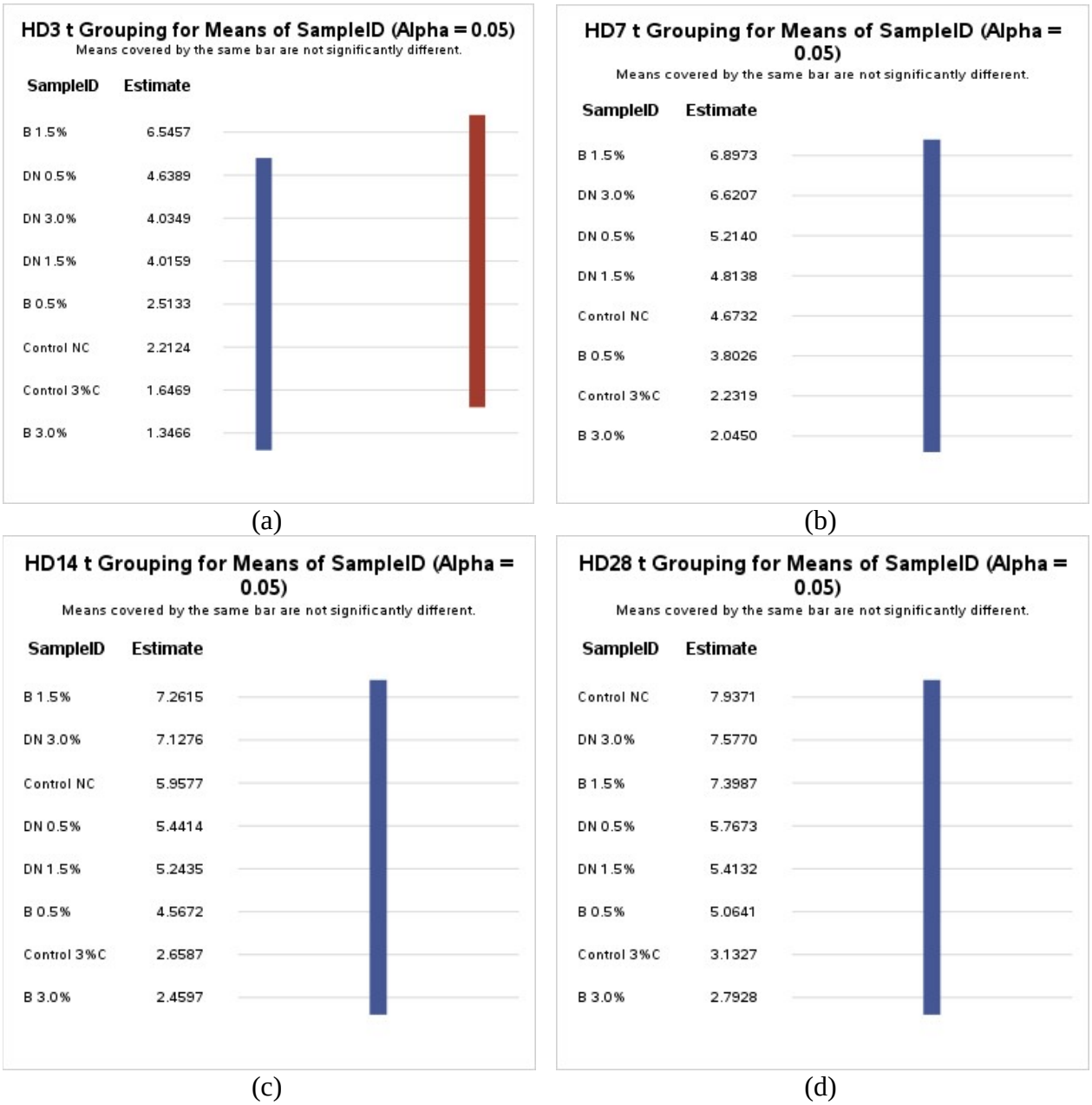

Figure 20. Fisher's LSD results for the normalized crack-healing efficiencies (%) for the bottom cracks on (a) day 3, (b) day 7, (c) day 14, and (d) day 28 of the wet-dry cycles.

The mean crack width reduction from the bottom cracks was also used as an indication of the degree of self-healing observed in each specimen group, shown in Figure 21. As expected, the mean crack width reduction increased over time for all specimen groups. However, the mean crack width reduction was significantly lower at the bottom cracks than at the side cracks, reaching up to 33 microns as opposed to the 93 microns after 28 wet-dry cycles. Unlike the trends shown from the observed healing at the side cracks, DN 3.0% was the only specimen group that had higher crack width reductions than Control NC. Thus, for the bottom cracks, the autogenous healing of concrete seemed to control the crack repair process, particularly since there were no significant differences between the healing efficiencies of each specimen group (per Figure 20).

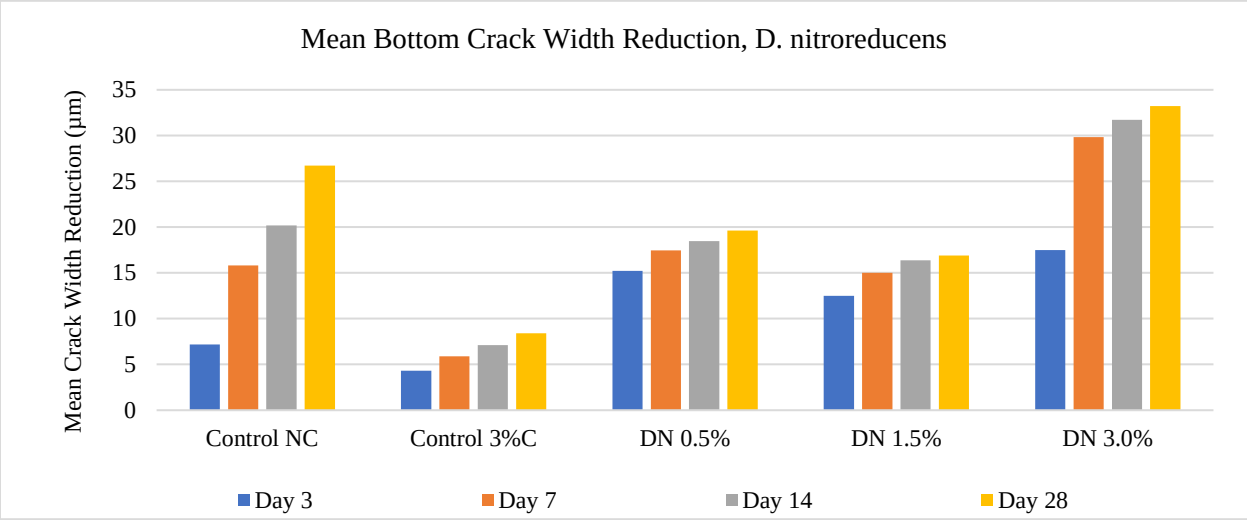

(a)

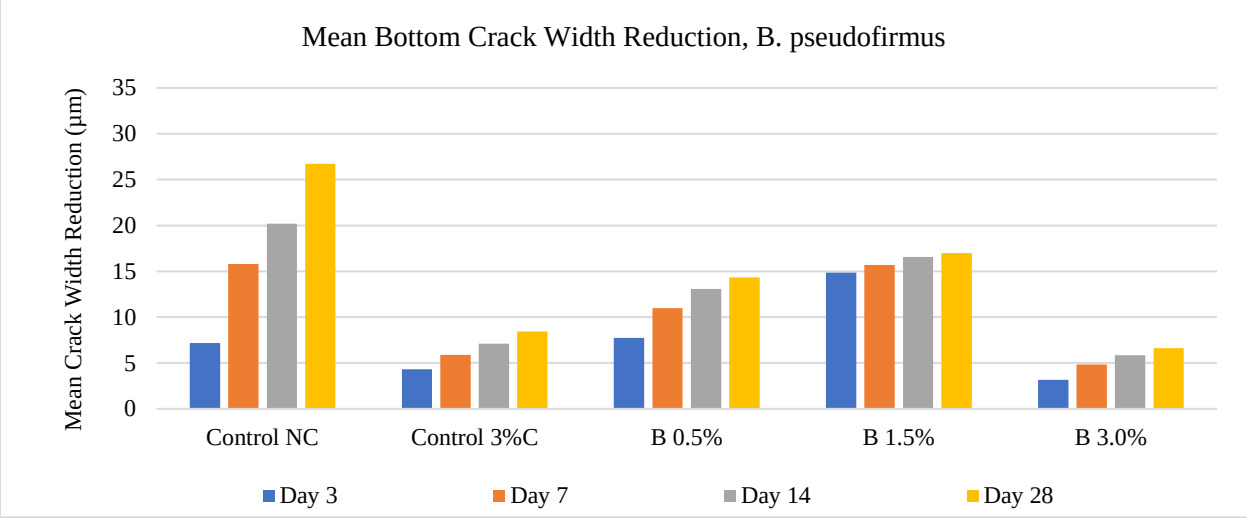

(b)

Figure 21. Mean bottom crack width reduction over time from (a) *D. nitroreducens* specimen groups; (b) *B. pseudofirmus* specimen groups.

5.6. Healing Product Characterization

SEM-EDS analysis confirmed that the healing crystals produced on top of the healing concrete beam cracks, from both the concrete samples with *B. pseudofirmus and D. nitroreducens* beads, are indeed calcium carbonate. A spot and area analysis with EDS were used to characterize the elemental composition of the healing products formed at the cracked surfaces, shown in Figure 22. The results showed high peaks of Carbon, Calcium, and Oxygen, which are the essential components of calcite ($CaCO_3$). This can confirm the presence of bacterial activity, as the self-healing reaction is based on microbial-induced calcite precipitation.

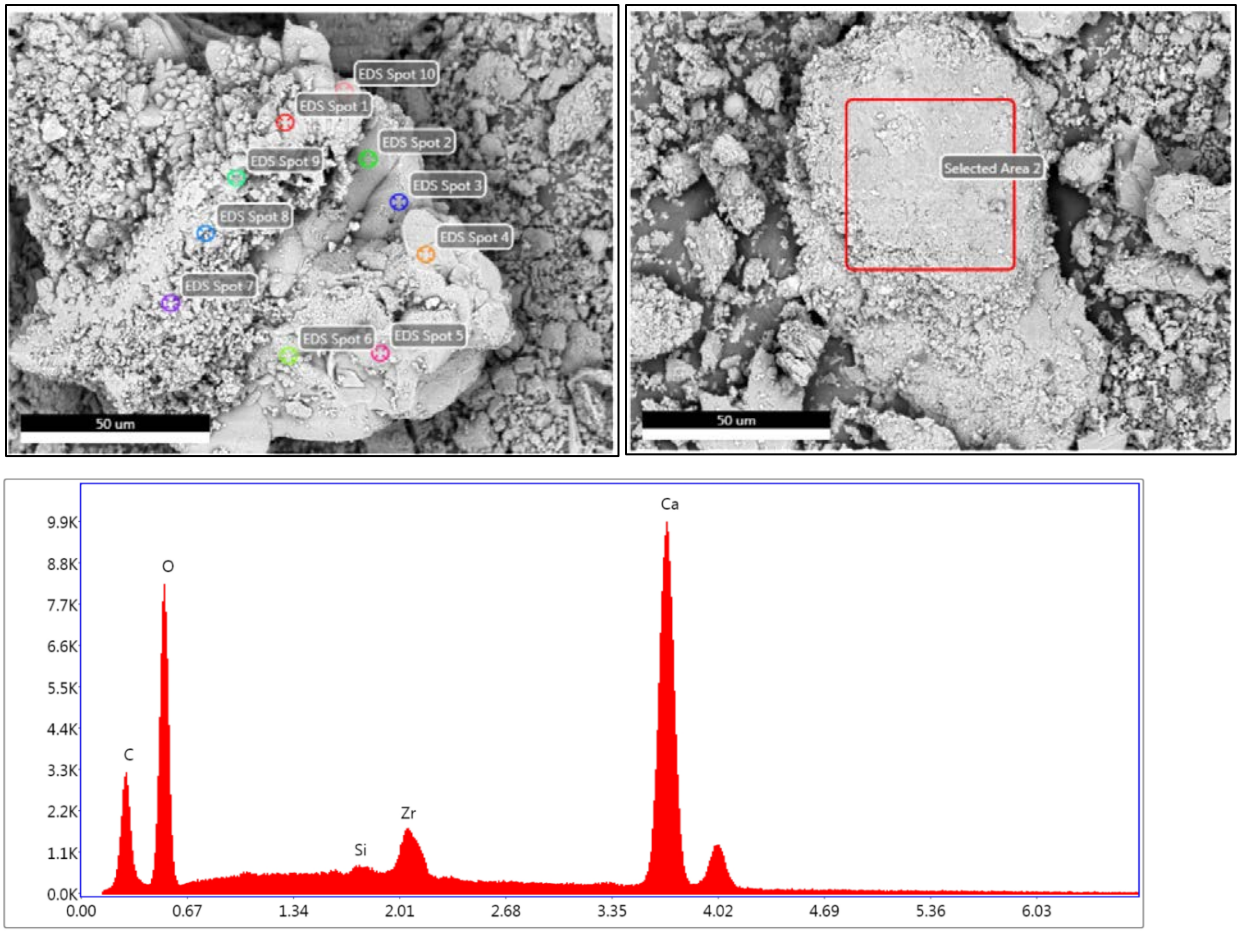

Figure 22. EDS analysis of healing products formed at cracked surfaces.

5.7. Surface Resistivity

The results of the surface resistivity test are interpreted using Table 8 to classify the chloride ion penetrability. The samples tested for surface resistivity had been initially damaged, and then allowed to heal after 28 wet/dry cycles.

Table 8. Chloride ion penetrability classification per surface resistivity readings (per AASHTO T 358).

Chloride Ion Penetrability	Surface Resistivity Reading (kΩ-cm)
High	< 12
Moderate	12 – 21
Low	21 – 37
Very Low	37 – 254
Negligible	> 254

The results show that high calcium alginate concentrations did have an influence on the chloride ion penetrability, as the only specimens that were ranked as ‘moderate’ had 3% of calcium alginate loading. However, it’s important to note that more pore water can result in lower surface resistivity values. Given that the calcium alginate beads can act as water reservoirs that could trigger or enhance the autogenous healing capacity of concrete, it is possible that this test method can yield inconclusive results. Future work should be done to assess the permeability of concrete (before

and after healing), as well as the ability of self-healing concrete to mitigate corrosion in steel reinforcement.

Table 9. Surface resistivity test results after 28 wet/dry cycles.

Sample ID	Surface Resistivity (kΩ-cm)	Chloride Ion Penetrability
Control NC	23	Low
Control 3%C	18	Moderate
DN 0.5%	25	Low
DN 1.5%	24	Low
DN 3.0%	20	Moderate
B 0.5%	27	Low
B 1.5%	26	Low
B 3.0%	16	Moderate

6. CONCLUSIONS

Self-healing concrete through encapsulated microbial agents was evaluated for its crack-sealing efficiency and stiffness recovery in polymer fiber-reinforced concrete beams and cylinders, respectively. The bacterial strains studied were *B. pseudofirmus* and *D. nitroreducens* and were encapsulated with calcium alginate beads via an extrusion dripping process.

The influence of the calcium alginate beads on the intrinsic mechanical properties of concrete was explored. In general, lower concentrations of alginate beads did not yield significant differences in compressive strength (at 0.5% by wt. of cement) and modulus of elasticity (at 0.5% and 1.5% by wt. of cement) than the control specimens with no alginate beads embedded.

After overloading the concrete cylinders to inflict damage (at 90% of their ultimate strength), the drop in modulus of elasticity was measured, and the samples were then allowed to heal in wet/dry cycles consisting of 8 hours of water immersion and 16 hours of air drying at a 50% RH room. The specimen groups with the highest calcium alginate concentrations resulted in higher increases in stiffness recovery. Interestingly, this observation also applied with the control specimens embedded with 3% calcium alginate beads without bacteria.

The self-healing efficiency was also monitored on cracked concrete beams over a period of 28 days for both the side cracks and bottom cracks. After measuring the side crack widths of damaged beams over time, it was evident that those samples containing alginate beads had superior self-healing efficiencies than the control samples without alginate beads (Control NC). However, it is important to note that the Control 3%C group (containing alginate beads with nutrients but no bacteria) also showed promising results in self-healing. This can be attributed to the fact that the alginate beads act as a reservoir that can further enhance the autogenous healing capability of concrete.

For the bottom cracks, however, there was minimal self-healing observed over time. There were no statistical differences in self-healing between all specimen groups, which suggests that the crack widths were too large for the alginate beads with and without bacteria to have an appreciable effect. These observations draw into question whether the influence of bacteria as sufficient to significantly enhance the self-healing process (with respect to stiffness recovery and crack sealing) based on this study's parameters.

Overall, further research is recommended to verify whether the promising results reported in the literature (relating to self-healing mortar) correlate with concrete proportionally. In addition, there is a need to explore the factors that can maximize the self-healing mechanism of bio concrete through MICP, whether an alternative encapsulation mechanism, nutrient selection, curing regime, or bacterial strain is desired.

REFERENCES

1. ASCE. *ASCE Infrastructure Report Card*. American Society of Civil Engineers. https://www.infrastructurereportcard.org/. Accessed Feb. 15, 2018.

2. Wu, M., B. Johannesson, and M. Geiker. A Review: Self-Healing in Cementitious Materials and Engineered Cementitious Composite as a Self-Healing Material. *Construction and Building Materials,* 2012. 28: 571-583.

3. Tziviloglou, E., V. Wiktor, H.M. Jonkers, and E. Schlangen. Bacteria-Based Self-Healing Concrete to Increase Liquid Tightness of Cracks. *Construction and Building Materials,* 2016. 122: 118-125.

4. Palin, D., D. Wiktor, and H.M. Jonkers. A Bacteria-Based Bead for Possible Self-Healing Marine Concrete Applications. *Smart Materials and Structure,* 2016. 25.

5. Souradeep, G. and H.W. Kua. Encapsulation Technology and Techniques in Self-Healing Concrete. *Journal of Materials in Civil Engineering,* 2016. 28(12): 04016165. DOI: 10.1061/(ASCE)MT.1943-5533.0001687

6. Jonkers, H.M., A. Thijssen, G. Muyzer, O. Copurogly, and E. Schlangen. Application of Bacteria as Self-Healing Agent for the Development of Sustainable Concrete. *Ecological Engineering,* 2010. 36: 230-235.

7. Wang, J., H. Soens, W. Vertstraete, and N. De Belie. Self-Healing Concrete by Use of Microencapsulated Bacterial Spores. *Cement and Concrete Research,* 2014a. 56: 139-152.

8. Wang, J., D. Snocek, W. Van Vlierberghe, W. Vertstraete, and N. De Belie. Application of Hydrogel Encapsulated Carbonate Precipitating Bacteria for Approaching a Realistic Self-Healing in Concrete. *Construction and Building Materials,* 2014b. 58: 110-119.

9. Wang, J., A. Mignon, D. Snoeck, V. Wiktor, N. Boon, and N. De Belie. Application of Modified-Alginate Encapsulated Carbonate Producing Bacteria in Concrete: A Promising Strategy for Crack Self-Healing. *Frontiers in Microbiology,* 2015. 6.

10. Silva, F. *Up-Scaling the Production of Bacteria for Self-Healing Concrete Application*. PhD Thesis, Ghent University, 2015.

11. Ersan, Y.C., E. Hernandez-Sanabria, N. De Belie, and N. Boon. Enhanced Crack Closure Performance of Microbial Mortar through Nitrate Reduction. *Cement and Concrete Composites,* 2016. 70: 159-170.

12. De Belie, N. Application of Bacteria in Concrete: A Critical Review. *RILEM Technical Letters,* 2016. 1: 56-61. DOI 10.21809/rilemtechlett.2016.14

13. Wiktor, V. and H.M. Jonkers. Quantification of Crack-Healing in Novel Bacteria-Based Self-Healing Concrete. *Cement and Concrete Composites,* 2011. 33: 763-70.

14. Wang, J., N. De Belie, and W. Verstraete. Diatomaceous Earth as a Protective Vehicle for Bacteria Applied for Self-Healing Concrete. *Journal of Industrial Microbiology and Biotechnology,* 2012. 39: 567-77.

15. Joshi, S., S. Goyal, A. Mukherjee, and M.S. Reddy. Microbial Healing of Cracks in Concrete: A Review. *Journal of Industrial Microbiology and Biotechnology*, 2017. 44: 1511-1525.

16. De Muynck, W., N. De Belie, and W. Verstraete. Microbial Carbonate Precipitation in Construction Materials: A Review. *Ecological Engineering*, 2010. 36: 118-136.

17. Beltran, M.G. and H.M. Jonkers. Crack Self-Healing Technology Based on Bacteria. *Journal of Ceramic Processing Research*, 2015. 16(1): 33-39.

18. Sharma, T.K., M. Alazhari, A. Heath, K. Paine, R.M. Cooper. Alkaliphilic *Bacillus* Species Show Potential Application in Concrete Crack Repair by Virtue of Rapid Spore Production and Germination Then Extracellular Calcite Formation. *Journal of Applied Microbiology*, 2017. 122: 1233-1244. DOI: 10.1111/jam.13421

19. Whelehan, M. *Encapsulator B-390/B-395 Pro Laboratory Guide*. BÜCHI Labortechnik AG, Flawil, Switzerland, 2014. https://www.johnmorrisgroup.com/Content/Attachments/150414/Encapsulator_Laboratory_Guide_en_A.pdf. Accessed Mar. 9, 2019.

20. Anbu P., C. Kang, Y. Shin, and J. So. Formations of Calcium Carbonate Minerals by Bacteria and its Multiple Applications: Review. *SpringerPlus*, 2016. 5:250. DOI: 10.1186/s40064-016-1869-2.

21. Seifan, M., A.K. Samani, and A. Berenjian. Bio-concrete: Next Generation of Self-Healing Concrete. *Applied Microbiology and Biotechnology*, 2016. 100: 2591-2602.

22. Dhami, N.K., S.M. Reddy, and A. Mukherjee. Biofilm and Microbial Applications in Biomineralized Concrete. *Advanced Topics in Biomineralization*, 2012. 137-164.

23. PCA. *Types and Causes of Concrete Deterioration*. Portland Cement Association, Skokie, IL, 2002.

24. Neville, A.M. *Properties of Concrete*. Pearson Higher Education (4th ed.), Prentice Hall, New Jersey, 1996.

25. Wang, J. *Self-Healing Concrete by Means of Immobilized Carbonate Precipitating Bacteria*. PhD Thesis, Ghent University, 2013.

26. Wang, J., H.M. Jonkers, N. Boon, and N. De Belie. *Bacillus sphaericus* LMG 22257 is Physiologically Suitable for Self-Healing Concrete. *Applied Microbiology and Biotechnology*, 2017. 101: 5101- 51144.

27. Ersan, Y.C., N. De Belie, and N. Boon. Microbially Induced CaCO3 Precipitation through Denitrification: An Optimization Study in Minimal Nutrient Environment. *Biochemical Engineering Journal*, 2015. 101: 108-118.

28. Kavazanjian, E. and I. Karatas. Microbiological Improvement of the Physical Properties of Soil. *International Conference on Case Histories in Geotechnical Engineering*, 2008. 1.

29. Van Paassen, L.A., C.M. Daza, M. Staal, D.Y. Sorokin. Potential Soil Reinforcement by Biological Denitrification. *Ecological Engineering*, 2010. 36: 168-175.

30. Zhu, T., C. Paulo, M.L. Merroun, M. Dittricha. Potential Application of Biomineralization by *Synechococcus* PCC8806 for Concrete Restoration. *Ecological Engineering*, 2015. 82: 459-468.

31. Justnes, H. *Calcium Nitrate as a Multifunctional Concrete Admixture*. SINTEF Technology and Society, Trondheim, Norway, 2015.

32. Berninger, T., B. Mitter, and C. Preininger. The Smaller, the Better? The Size Effect of Alginate Beads Carrying Plant Growth-Promoting Bacteria for Seed Coating. *Journal of Microencapsulation,* 2016. 33(2): 127.

33. Devan Chemicals NV. WO 2010/142401. *Microcapsules Containing Microorganisms*. 2010. Patent No. AU2010257855.

34. Semba, D. and A. Trusek-Hołownia. Generation of Homo- and Heterogeneous Microcapsules and Their Application. *Technical Transactions: Mechanics,* 2017. 197-208. DOI: 10.4467/2353737XCT.17.060.6371.

35. Lee, B., P. Ravindra, and E. Chan. Size and Shape of Calcium Alginate Beads Produced by Extrusion Dripping. *Chemical Engineering Technology*, 2013. 36(10): 1627-1642. DOI: 10.1002/ceat.201300230

36. Seifan M., A.K. Samani, S. Hewitt, and A. Berenjian. The Effect of Cell Immobilization by Calcium Alginate on Bacterially Induced Calcium Carbonate Precipitation. *Fermentation*, 2017. 3: 57. DOI: 10.3390/fermentation3040057.

37. Zhang, J., Y. Gao, Y. Han, W. Sun. Shrinkage and Interior Humidity of Concrete under Dry-Wet Cycles. *Drying Technology*, 2012. 30: 583-596. DOI: 10.1080/07373937.2011.653614.

38. Hassan, M.M, J. Milla, T. Rupnow, M. Al-Ansari, and W.H. Daly. Microencapsulation of Calcium Nitrate for Concrete Applications. *Transportation Research Record, Journal of the Transportation Research Board*, 2016. 2577(1). DOI: 10.3141/2577-02.

APPENDIX

Table A1. Average bottom crack widths from the 3 beam replicates for each specimen on day 0 to 28 of the wet/dry cycles along with the corresponding healing efficiencies.

Sample ID	Sample No.	Class	Concentration (% by wt. of cement)	Crack Width (microns)					Healing Efficiencies (%)			
				Day 0	Day 3	Day 7	Day 14	Day 28	Day 3	Day 7	Day 14	Day 28
Control 3%C	1	Control w 3% beads	3.00%	249.93	246.04	245.91	244.75	244.06	1.56	1.61	2.07	2.35
Control 3%C	2	Control w 3% beads	3.00%	222.47	217.57	215.03	214.45	213.03	2.20	3.34	3.60	4.24
Control 3%C	3	Control w 3% beads	3.00%	354.59	350.40	348.41	346.44	344.64	1.18	1.74	2.30	2.81
Control NC	1	Control	0	380.51	377.56	362.15	355.41	355.49	0.78	4.83	6.60	6.58
Control NC	2	Control	0	308.05	295.54	287.51	280.63	276.79	4.06	6.67	8.90	10.15
Control NC	3	Control	0	337.60	331.52	329.07	329.58	313.67	1.80	2.53	2.38	7.09
B 0.5%	1	B. Pseudofirmus	0.50%	266.20	262.06	260.40	259.34	258.54	1.56	2.18	2.58	2.88
B 0.5%	2	B. Pseudofirmus	0.50%	205.26	202.31	197.73	195.64	193.90	1.44	3.67	4.69	5.53
B 0.5%	3	B. Pseudofirmus	0.50%	353.38	337.31	333.73	330.63	329.42	4.55	5.56	6.44	6.78
B 1.5%	1	B. Pseudofirmus	1.50%	279.24	275.05	274.61	273.56	273.25	1.50	1.66	2.03	2.15
B 1.5%	2	B. Pseudofirmus	1.50%	301.39	281.52	280.36	279.54	278.60	6.59	6.98	7.25	7.56
B 1.5%	3	B. Pseudofirmus	1.50%	177.67	157.16	156.25	155.46	155.48	11.54	12.06	12.50	12.49
B 3.0%	1	B. Pseudofirmus	3.00%	278.19	276.77	275.68	274.82	274.78	0.51	0.90	1.21	1.23
B 3.0%	2	B. Pseudofirmus	3.00%	249.47	247.71	246.26	245.72	244.92	0.71	1.29	1.50	1.82
B 3.0%	3	B. Pseudofirmus	3.00%	222.75	216.46	213.96	212.36	210.88	2.82	3.95	4.66	5.33
DN 0.5%*	1	D. Nitroreducens	0.50%	455.90	445.88	442.63	440.73	439.61	2.20	2.91	3.33	3.57
DN 0.5%	2	D. Nitroreducens	0.50%	N/A	N/A	N/A	N/A	N/A	N/A	N/A	N/A	N/A
DN 0.5%	3	D. Nitroreducens	0.50%	288.14	267.74	266.48	266.37	265.20	7.08	7.52	7.56	7.96
DN 1.5%	1	D. Nitroreducens	1.50%	317.16	314.76	310.01	307.09	307.47	0.76	2.25	3.18	3.06
DN 1.5%	2	D. Nitroreducens	1.50%	308.46	286.71	285.89	285.48	284.10	7.05	7.32	7.45	7.90
DN 1.5%	3	D. Nitroreducens	1.50%	314.16	300.84	298.86	298.12	297.55	4.24	4.87	5.11	5.29
DN 3.0%	1	D. Nitroreducens	3.00%	498.99	457.57	423.15	420.03	418.89	8.30	15.20	15.82	16.05
DN 3.0%	2	D. Nitroreducens	3.00%	308.22	303.51	301.46	300.72	297.79	1.53	2.19	2.43	3.38
DN 3.0%	3	D. Nitroreducens	3.00%	277.72	271.40	270.86	269.04	268.57	2.28	2.47	3.13	3.29

*Only two replicates used for specimen DN 0.5%, due to unintended, substantially large crack widths produced during the damage phase.

Table A2. Average side crack widths from the 3 beam replicates for each specimen on day 0 to 28 of the wet/dry cycles along with the corresponding healing efficiencies.

Sample ID	Sample No.	Class	Concentration (% by wt. of cement)	Crack Width (microns)					Healing Efficiencies (%)			
				Day 0	Day 3	Day 7	Day 14	Day 28	Day 3	Day 7	Day 14	Day 28
Control 3%C	1	Control w 3% beads	3.00%	105.45	47.98	36.80	26.42	21.90	54.50	65.10	74.95	79.23
Control 3%C	2	Control w 3% beads	3.00%	111.26	70.55	55.70	47.51	43.93	36.59	49.94	57.30	60.52
Control 3%C	3	Control w 3% beads	3.00%	144.32	106.82	71.17	56.23	52.35	25.98	50.69	61.04	63.73
Control NC	1	Control	0	182.37	168.50	113.21	102.02	101.27	7.61	37.92	44.06	44.47
Control NC	2	Control	0	131.11	107.49	81.73	75.42	74.77	18.02	37.66	42.48	42.97
Control NC	3	Control	0	207.76	205.31	179.87	167.54	162.53	1.18	13.42	19.36	21.77
B 0.5%	1	B. Pseudofirmus	0.50%	127.81	102.69	81.31	76.36	72.43	19.65	36.38	40.26	43.33
B 0.5%	2	B. Pseudofirmus	0.50%	110.95	86.34	62.35	50.36	48.29	22.18	43.80	54.61	56.48
B 0.5%	3	B. Pseudofirmus	0.50%	166.68	115.77	80.58	62.20	58.14	30.54	51.66	62.68	65.12
B 1.5%	1	B. Pseudofirmus	1.50%	132.12	107.13	91.89	91.20	85.96	18.91	30.45	30.97	34.94
B 1.5%	2	B. Pseudofirmus	1.50%	134.95	103.68	79.95	80.49	76.56	23.17	40.76	40.36	43.27
B 1.5%	3	B. Pseudofirmus	1.50%	94.61	67.50	65.61	59.42	55.69	28.65	30.65	37.19	41.14
B 3.0%	1	B. Pseudofirmus	3.00%	142.24	99.78	93.83	86.05	84.81	29.85	34.04	39.51	40.38
B 3.0%	2	B. Pseudofirmus	3.00%	129.31	73.06	58.32	53.37	51.12	43.50	54.90	58.73	60.47
B 3.0%	3	B. Pseudofirmus	3.00%	107.97	64.83	55.15	36.16	34.10	39.96	48.92	66.51	68.42
DN 0.5%	1	D. Nitroreducens	0.50%	160.29	114.13	88.79	54.18	53.08	28.80	44.61	66.20	66.89
DN 0.5%*	2	D. Nitroreducens	0.50%	N/A	N/A	N/A	N/A	N/A	N/A	N/A	N/A	N/A
DN 0.5%	3	D. Nitroreducens	0.50%	140.50	87.66	67.82	68.62	67.72	37.61	51.73	51.16	51.80
DN 1.5%	1	D. Nitroreducens	1.50%	151.58	95.32	80.50	76.32	74.13	37.12	46.89	49.65	51.10
DN 1.5%	2	D. Nitroreducens	1.50%	165.81	107.58	90.88	78.59	77.29	35.12	45.19	52.60	53.39
DN 1.5%	3	D. Nitroreducens	1.50%	112.65	74.30	54.15	47.05	44.29	34.04	51.93	58.23	60.68
DN 3.0%	1	D. Nitroreducens	3.00%	250.37	182.84	158.13	137.89	135.07	26.97	36.84	44.93	46.05
DN 3.0%	2	D. Nitroreducens	3.00%	136.57	84.35	52.20	39.60	37.42	38.24	61.78	71.00	72.60
DN 3.0%	3	D. Nitroreducens	3.00%	126.78	74.26	65.94	63.81	62.22	41.43	47.99	49.67	50.92

*Only two replicates used for specimen DN 0.5%, due to unintended, substantially large crack widths produced during the damage phase.